# Quasiparticle current along the *c* axis in junctions involving *d*-wave superconductors partially gapped by charge density waves

Alexander M. Gabovich,[1,*] Mai Suan Li,[2,†] Henryk Szymczak,[2,‡] and Alexander I. Voitenko[1,§]
[1]*Institute of Physics, Nauka Ave. 46, Kyiv 03680, Ukraine*
[2]*Institute of Physics, Al. Lotników 32/46, PL-02-668 Warsaw, Poland*
(Received 1 July 2015; published 24 August 2015)

Quasiparticle tunnel current either between identical *d*-wave superconductors partially gapped by charge density waves (SCDWs) or between an SCDW and a normal metal was calculated. The cases of unidirectional and checkerboard CDWs were considered. The tunnel conductance was found in both cases to possess a number of peculiarities, which cannot be described by introducing a single combined gap. The results are in qualitative agreement with experimental data obtained for a number of cuprates by the scanning tunnel spectroscopy, intrinsic-tunneling, and break-junction measurements. The difference between the experiment and the theory seems to stem from the spread of gap values occurring due to the intrinsic spatial inhomogeneity of nonstoichiometric oxides and reflected in the cuprate tunnel spectra.

DOI: 10.1103/PhysRevB.92.054512 PACS number(s): 71.45.Lr, 74.55.+v, 74.81.−g

## I. INTRODUCTION

Charge density waves (CDWs), which have recently been observed directly in a number of high-$T_c$ oxides [1–6], have been suspected long ago to induce pseudogapping in the electron density of states (DOS) [6–13]. Earlier, CDWs coexisting and competing with superconductivity were indirectly detected in hole-doped oxides by elastic and inelastic x-ray scattering [3–5,14–24], Raman scattering [25], scanning tunnel microscopy (STM) [22,23,26–28], nuclear magnetic resonance (NMR) [29–31], angle-resolved photoemission (ARPES) measurements [22,32,33], ultrafast pump-probe spectroscopy [11,34], sound velocity studies [35], Hall resistance [36], and magnetoresistivity oscillations [37]. A charge ordering similar to that in hole-doped cuprates was recently found in the electron-doped compound $Nd_{2-x}Ce_xCuO_4$ by resonant x-ray scattering [38]. On the basis of this evidence and related experimental data, we identify the CDW-related gap with the pseudogap, although the latter might be, in principle, a more complex phenomenon including, e.g., some kind of fluctuating Cooper pairs as well [6,39]. There is also a viewpoint that the real intertwining involves superconductivity and pair-density waves (PDWs), the observed CDWs being a kind of composite ordering induced by the former two basic phenomena [13]. In another scenario [40,41], CDWs and PDWs coexist, possess the same momentum $\mathbf{Q}$, and compete with superconductivity in the same manner as is proposed here.

Dielectric energy gaps observed by the quasiparticle tunnel spectroscopy and associated with the DOS depletion induced by Peierls-like electron-hole correlations have the forms [42] similar to those induced by the Cooper pairing in tunnel spectra [43]. (The similarity is due to the applicability of the semiconducting model to superconducting tunnel spectra because of the disappearance of coherence factors from the final result [44].) Therefore, the tunnel conductance in partially CDW-gapped superconductors should demonstrate properties revealing both kinds of many-body phenomena. The corresponding calculations of the dynamic conductance [the differential current-voltage characteristic (CVC)] $G(V) \equiv dJ/dV$, where $J$ is the quasiparticle tunnel current and $V$ is the bias voltage, were performed for both *s*-wave [45–50] and *d*-wave [51] superconductors partially gapped by CDWs. In this work, we present a detailed analysis of the problem in two important specific cases: (i) a nonsymmetric junction between a *d*-wave single-crystalline superconductor partially gapped by CDWs (SCDW) and a normal (metal) electrode (N), with the *c* axis of the SCDW being oriented perpendicularly to the junction plane; and (ii) a symmetric junction between two identical SCDWs, with their *c* axes also being directed normally to the junction. We employed the two-dimensional model of the electron spectrum in the SCDW and analyzed the bidirectional (checkerboard) and unidirectional (stripe) CDW patterns, both being appropriate to high-$T_c$ oxides [10,51–54].

In this work, we analyze spatially homogeneous SCDWs. Strictly speaking, this is not the case for high-$T_c$ oxides because of their intrinsic nonstoichiometric nature [54–59]. Nevertheless, this model describes the main features of the corresponding tunnel spectra, being an unavoidable basic stage in the development of the theory. The absence of the intrinsic SCDW parameter spread—the spread would ultimately result in the smearing of $G(V)$ peculiar points—allows the feature points in the quasiparticle spectrum related to the singularities of $G(V)$s to be determined. Besides, the role of the temperature $T$ in the $G(V)$ evolution can be discerned more clearly. Note also that some authors [59,60] associate the pseudogap phenomenon with the spatial inhomogeneity.

## II. DESCRIPTION OF COMPETING SUPERCONDUCTING AND CDW ORDER PARAMETERS

### A. Basic relations

The model of the two-dimensional electron spectrum gapped by both the CDW (partial gapping at $T < T_s$) and *d*-wave superconducting pairings (at $T < T_c$) is adopted [7,51,52]. Which of $T_c$ or $T_s$ is higher depends on the

*gabovich@iop.kiev.ua
†masli@ifpan.edu.pl
‡szymh@ifpan.edu.pl
§voitenko@iop.kiev.ua

 

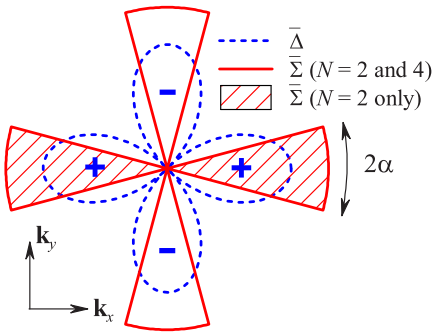


FIG. 1. (Color online) Schematic diagrams for the parent order parameters of the $d$-wave superconductor partially gapped by charge-density waves (CDWs) at the temperature $T = 0$. The dashed curve describes the alternating-sign $\bar{\Delta}(\theta)$ function for the parent $d$-wave superconductor (dBCS), and the solid curve the $\bar{\Sigma}(\theta)$ dependence for the parent partially gapped metal. The angle $\theta$ is reckoned counterclockwise from the $\mathbf{k}_x$ direction in the momentum space. The relative orientation of the $\bar{\Delta}(\theta)$ and $\bar{\Sigma}(\theta)$ profiles correlates with that for cuprates (the $d_{x^2-y^2}$-wave symmetry). There are $N = 4$ CDW-gapped Fermi surface (FS) sections in the case of checkerboard CDW pattern, and $N = 2$ (hatched) gapped sections in the case of unidirectional CDWs. $2\alpha$ is the angular width of each CDW sector.

SCDW parameters. In the framework of this approach, CDWs are a consequence of the partial Fermi surface (FS) nesting and are generated by either the electron-phonon (the Peierls insulator) or Coulomb (the excitonic insulator) interaction. As comes about from the experiment, electronic CDWs in cuprates are accompanied by periodic lattice distortions [1,3–5], contrary to what is sometimes asserted [61]. The approximate two dimensionality of the electron spectrum is a consequence of the layered crystal structure inherent to high-$T_c$ oxides.

Hence, the gapped spectrum in the low-$T$ phase of the SCDW is a result of the interplay between two pairing mechanisms: the nonisotropic electron-electron attraction, which is considered here as a four-fermion phenomenological interaction, and the isotropic (*within the dielectrized FS sections*; see below) electron-hole one (Fig. 1).

For completeness, let us consider the SCDW model in brief. The mean-field Hamiltonian has the form,

$$H = H_{\rm kin} + H_{\rm BCS} + H_{\rm CDW}, \tag{1}$$

where

$$H_{\rm kin} = \sum_{\mathbf{k},\sigma=\uparrow,\downarrow} \sum_{i=d,nd} \xi_i(\mathbf{k}) a^\dagger_{i,\mathbf{k},\sigma} a_{i,\mathbf{k},\sigma}, \tag{2}$$

$$H_{\rm BCS} = \sum_{\mathbf{k}} \bar{\Delta}(\mathbf{k}) \sum_{i=d,nd} a^\dagger_{i,\mathbf{k},\uparrow} a^\dagger_{i,-\mathbf{k},\downarrow} + \text{c.c.}, \tag{3}$$

$$H_{\rm CDW} = \sum_{\mathbf{k},\sigma=\uparrow,\downarrow} \sum_{i=d} \bar{\Sigma}(\mathbf{k}) a^\dagger_{i,\mathbf{k},\sigma} a_{i,\mathbf{k}+\mathbf{Q},\sigma} + \text{c.c.} \tag{4}$$

Here, $\xi_i(\mathbf{k})$ is the initial quasiparticle spectrum; the momentum-dependent $d$-wave superconducting, Bardeen-Cooper-Schrieffer-like (BCS-like) order parameter, $\bar{\Delta}(\mathbf{k})$, and the CDW one, $\bar{\Sigma}(\mathbf{k})$, are specified below; $a^\dagger$ and $a$ are the creation and annihilation operators, respectively; $\sigma$ is the quasiparticle spin projection, $\mathbf{Q}$ is the CDW vector, and the notations "d" and "nd" were introduced for the dielectrized and nondielectrized FS sections, respectively.

If the Cooper pairing had been absent, the low-$T$ state would have been a parent CDW phase (a metal partially gapped by CDWs). The partial gapping means that only a finite fraction of the FS is gapped (to distinguish this gapping from the superconducting one, it will be referred to as dielectrization). In accordance with observations for various cuprates, the arrangement of dielectrized sections on the FS may be characterized as either checkerboard (biaxial, the number of the CDW sectors $N = 4$) or unidirectional (stripe, $N = 2$) (see Fig. 1 ) [1,9,62]. Biaxial CDWs does not violate the $C_4$ crystal symmetry, contrary to uniaxial CDWs (stripes), the appearance of which reveals the nematic or smectic rotational symmetry breaking. The latter phenomenon was observed in cuprates [63–66], as well as iron-based superconductors [67–69], and, in general, may be due to various microscopic reasons [70–76]. For instance, it might be intimately linked to the intrinsic disorder in nonstoichiometric crystals [77,78].

The CDW complex order parameter $\Sigma_0(T)e^{i\varphi}$ (here, $\varphi$ is the CDW phase) is constant (the $s$-wave symmetry) within each of four (biaxial CDW) or two (uniaxial CDW) Fermi surface (FS) hot-spot sectors. The latter are nested in pairs and oriented crosswise, also in pairs, along the lattice $\mathbf{k}_x$ and $\mathbf{k}_y$ axes in the momentum space. Each of the sectors has the angular width $2\alpha$. We identify the CDW ordering with the pseudogap one, although it might happen that CDWs are only related to the pseudogap phase, with the latter covering a larger area than the former in the cuprate $T$-$y$ phase diagram, where $y$ is the doping parameter [12]. The theory shows that if the parent CDW metal is characterized by the order parameter magnitude $\Sigma_0(0)$ at $T = 0$, then, up to the critical temperature $T_{s0} = \frac{\gamma}{\pi}\Sigma_0(0)$, where $\gamma = 1.78\ldots$ is the Euler constant, and the Boltzmann constant $k_B = 1$, the dependence,

$$\Sigma_0(T) = \Sigma_0(0)\text{Mü}_s(T/T_{s0}), \tag{5}$$

is satisfied, where $\text{Mü}_s(x)$ is the reduced [i.e., $\text{Mü}_s(0) = 1$] standard ($s$-wave) Mühlschlegel dependence [79]. For further consideration, let us introduce the angle $\theta$ in the two-dimensional momentum ($\mathbf{k}$) plane that describes a direction reckoned from the $\mathbf{k}_x$ one. Then, to describe the "profile" $\bar{\Sigma}_0(T,\mathbf{k})$, or $\bar{\Sigma}_0(T,\theta)$, over the whole FS, it is convenient to use the angular factor $f_\Sigma(\theta)$, which is equal to 1 inside and 0 outside each sector. Then, $\bar{\Sigma}_0(T,\theta)$ can be factorized as follows:

$$\bar{\Sigma}_0(T,\theta) = \Sigma_0(T) f_\Sigma(\theta). \tag{6}$$

In the framework of the model concerned, the function $f_\Sigma(\theta)$ is supposed to be independent of $T$ and the electron-hole pairing strength, which is in agreement with the experiment [80,81]. At the same time, the parameter $\alpha$ can be influenced by a number of external factors, e.g., doping or pressure. Such a picture correlates, in particular, with the ARPES data for $Bi_2Sr_2CaCu_2O_{8+\delta}$ [80], according to which the CDW sectors shrink for overdoped compositions.

On the other hand, if the CDW pairing had been switched off, we would have obtained a parent BCS $d_{x^2-y^2}$-wave superconductor (dBCS) [82] characterized by the superconducting order parameter $\Delta_0(0)$ at $T = 0$ and with the lobes of the

latter also oriented in the $\mathbf{k}_x$ and $\mathbf{k}_y$ directions, i.e., in the same (antinodal) directions as the bisectrices of CDW sectors (Fig. 1). In this case, the "profile" $\bar{\Delta}_0(T,\theta)$ of nonzero $\Delta_0$ in the $\mathbf{k}$ space spans the whole FS. It can also be factorized,

$$\bar{\Delta}_0(T,\theta) = \Delta_0(T) f_\Delta(\theta), \tag{7}$$

using the angular factor,

$$f_\Delta(\theta) = \cos 2\theta. \tag{8}$$

Below $T_{c0} = \frac{\gamma\sqrt{e}}{2\pi}\Delta_0(0)$, where e is the base of natural logarithms,

$$\Delta_0(T) = \Delta_0(0)\text{Mü}_d(T/T_{c0}), \tag{9}$$

where $\text{Mü}_d(x)$ is the reduced ($\text{Mü}_d(0) = 1$) superconducting order parameter dependence in the case of $d$-wave pairing [82]. The function $f_\Delta(\theta)$, similarly to $f_\Sigma(\theta)$, is also considered to be independent of $T$ and the Cooper pairing strength.

When both interactions are switched on and coexist, they compete for the same quasiparticle states at the Fermi surface. This mutually detrimental interplay leads to a drastic difference of the actual $\Sigma(T)$ and $\Delta(T)$ functions from the parent ones—$\Sigma_0(T)$ and $\Delta_0(T)$, respectively—in the interval of their coexistence [8,83]. The relevant self-consistent set of equations, which is to be solved to determine $\Sigma(T)$ and $\Delta(T)$ for the given set of the input model parameters [as such, $\Delta_0(0)$, $\Sigma_0(0)$—for brevity, they are denoted below as $\Delta_0$ and $\Sigma_0$, respectively—$\alpha$, and $N$ are selected] have the form [7,8,83],

$$\int_{-\alpha}^{\alpha} I_M(\sqrt{\Sigma^2 + \Delta^2\cos^2 2\theta}, T, \Sigma_0)d\theta = 0, \tag{10}$$

$$\int_{-\alpha}^{\alpha} I_M(\sqrt{\Sigma^2 + \Delta^2\cos^2 2\theta}, T, \Delta_0\cos 2\theta)\cos^2 2\theta d\theta + \int_{\alpha}^{\Omega-\alpha} I_M(\Delta\cos 2\theta, T, \Delta_0\cos 2\theta)\cos^2 2\theta d\theta = 0, \tag{11}$$

where

$$I_M(\Delta, T, \Delta_0) = \int_0^\infty \left(\frac{1}{\sqrt{\xi^2+\Delta^2}}\tanh\frac{\sqrt{\xi^2+\Delta^2}}{2T} - \frac{1}{\sqrt{\xi^2+\Delta_0^2}}\right)d\xi \tag{12}$$

is the Mühlschlegel integral of the BCS theory. The angle $\Omega$ equals $\pi$ for $N = 2$ and $\frac{\pi}{2}$ for $N = 4$. Now, neither of the order parameters can be described by the function $\text{Mü}_s(T/T_c)$ or $\text{Mü}_d(T/T_s)$. To be more specific, there may arise intervals where either of the order parameters vanishes; only within such intervals the other order parameter keeps its "parent" $T$ dependence. Accordingly, the lowest of the critical temperatures $T_{c0}$ or $T_{s0}$ changes to the corresponding, even lower value, $T_c$ or $T_s$, respectively. It usually comes about that in cuprates, as well as in other existing CDW superconductors, $T_{c0} < T_{s0}$ [7,84]. In our model, for generality, the ratio between $T_{c0}$ and $T_{s0}$ can be arbitrary. Besides, at some $[\Delta_0, \Sigma_0, \alpha, N]$ combinations, the phenomenon of the $\Sigma(T)$ reentrance may appear consisting in that $\Sigma(T) \neq 0$ within a certain interval $0 < T_r < T < T_s$ [7,8,83].

As a result, a nontrivial combined gap,

$$\bar{D}(T,\theta) = \sqrt{\Sigma^2(T) + \bar{\Delta}^2(T,\theta)},$$

arises on the dielectrized (d) FS sections, and the gap $|\bar{\Delta}(T,\theta)|$ exists on the nondielectrized (nd) ones. Making use of the functions $f_\Delta(\theta)$ and $f_\Sigma(\theta)$ once more, the profile of the resulting gap over the whole FS (the gap rose) can be written in the form,

$$\bar{D}(T,\theta) = \sqrt{\bar{\Sigma}^2(T,\theta) + \bar{\Delta}^2(T,\theta)}, \tag{13}$$

where

$$\bar{\Delta}(T,\theta) = \Delta(T) f_\Delta(\theta), \tag{14}$$

$$\bar{\Sigma}(T,\theta) = \Sigma(T) f_\Sigma(\theta). \tag{15}$$

Note that in the adopted approach the CDW wave vector $\mathbf{Q}$ falls out of thermodynamics and does not enter the system of integral equations for the relevant order parameters [7,8,83]. Therefore, any effects of the transition between commensurate and incommensurate CDWs are not included into consideration. We have not enough experimental evidence to examine such a possibility for cuprates. Nevertheless, those effects might be important, in principle, and the same wave vector $\mathbf{Q}$ might characterize the Cooper pairing leading in this case to an incommensurate pair-density wave. The competition between CDWs and superconductivity in the framework of this model has been examined recently [85,86].

A quite different $t - J$ model with both order parameters having $d$-wave symmetry was suggested earlier while considering $c$-axis quasiparticle tunneling [87]. The corresponding results for the electron density of states and the tunnel conductance $G(V)$ are substantially different from those obtained in this work.

### B. Representative parameter sets

The problem can be formalized further and the number of problem parameters can be reduced by normalizing the relevant energies by $\Delta_0$. Then, the set of problem parameters is reduced to $[\sigma_0, \alpha, N]$, where $\sigma_0 = \Sigma_0/\Delta_0$ evaluates the ratio between the electron-hole and Cooper pairing strengths. In Fig. 2(a), the $\sigma_0 - \alpha$ phase diagram of the SCDW when the relative orientation of the superconducting and CDW order parameters in the momentum space corresponds to Fig. 1 (i.e., in the case of $d_{x^2-y^2}$-wave pairing symmetry) and at $T = 0$ is exhibited [83]. In this work we consider how CDWs affect the tunnel spectra of $d$-wave superconductors and assume the Cooper pairing to be the basic one. We implement this assumption by putting $\Delta_0 = 1$ in all further calculations. Then, Fig. 2(a) can also be regarded as the $\Sigma_0 - \alpha$ phase diagram for the SCDW with $\Delta_0 = 1$ at $T = 0$.

The states to the right of the solid curve (the area marked as SCDW) are characterized by the temperature dependencies of their order parameters $\Delta(T)$ and $\Sigma(T)$ like those exhibited in Fig. 2(b). In the lower half of the plane ($0^\circ \leqslant \alpha \leqslant 45^\circ$), the phase diagrams for the checkerboard ($N = 4$) and unidirectional ($N = 2$) CDW configurations coincide. At the same time, the difference between those two cases in the common part of the phase diagram consists in that the corresponding

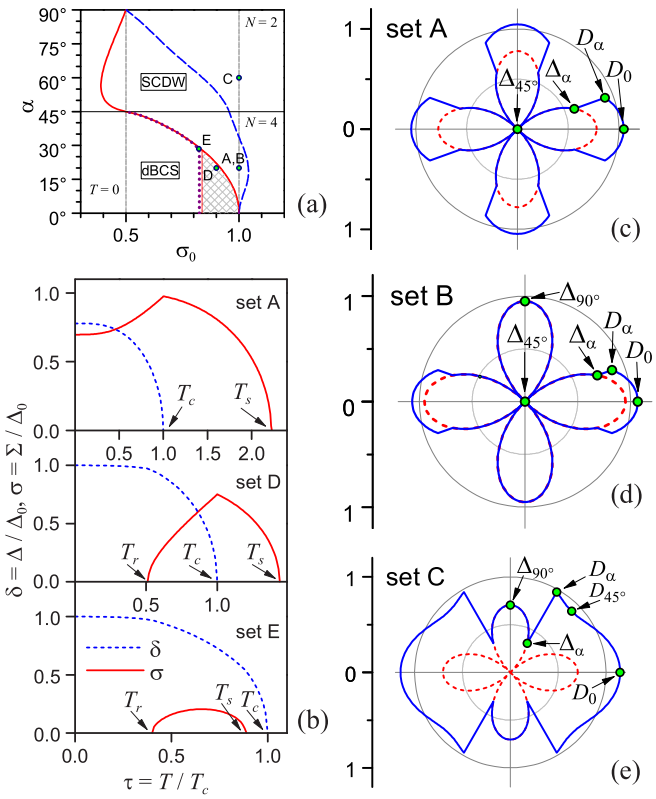


FIG. 2. (Color online) (a) Phase diagram $\sigma_0 - \alpha$ for the partially CDW-gapped $d$-wave superconductor (SCDW) at the temperature $T = 0$. Here, $\sigma_0 = \Sigma_0/\Delta_0$, where $\Sigma_0$ and $\Delta_0$ are the magnitudes of the zero-$T$ parent order parameters. The upper area ($\alpha > 45°$) makes sense only for $N = 2$, whereas the lower one is the same for $N = 4$ and $N = 2$. The solid curve separates the region where the SCDW is the dBCS from the region where superconductivity and CDWs coexist. In the hatched region between the solid and dotted boundaries, the CDW-reentrance phenomenon takes place at $T > 0$. Concerning representative points A–E and the dashed curve, see explanations in the text. (b) Possible types of $\delta(\tau)$ and $\sigma(\tau)$ dependencies for various SCDW parameter sets. Here, $\delta = \Delta/\Delta_0$ and $\sigma = \Sigma/\Delta_0$ are normalized superconducting $\Delta$, and dielectric $\Sigma$, actual order parameters, and $\tau = T/T_c$ is the temperature normalized by the actual superconducting critical temperature $T_c$. $T_r$ and $T_s$ denote the temperature interval of CDW existence. (c)–(e) Gap roses in the momentum space for the SCDWs (solid curves) and the relative dBCSs (dashed curves; see explanations in the text) corresponding to parameter sets A–C [see (a)]. The feature points are indicated (see notations in the text).

values of $\Delta$ and $\Sigma$ differ in pairs. Therefore, the relevant CVCs vary substantially.

For the purpose of illustration, three characteristic parameter sets were chosen in the SCDW area: set A ($N = 4$, $\Delta_0 = 1, \Sigma_0 = 1, \alpha = 20°$), set B ($N = 2, \Delta_0 = 1, \Sigma_0 = 1, \alpha = 20°$), and set C ($N = 2$, $\Delta_0 = 1, \Sigma_0 = 1$, $\alpha = 60°$). In the phase diagram [Fig. 2(a)], they are marked by the corresponding points. Below, they will be considered as "representative" ones, i.e., their CVCs will be regarded as basic while analyzing the effect of changing $\sigma_0$, $\alpha$, or $T$ separately. The difference between sets A, B, and C is illustrated by their gap roses at $T = 0$ (see Figs. 2(c)–2(e), respectively), whereas their $\Delta(T)$ and $\Sigma(T)$ dependencies are similar [see set A in Fig. 2(b)]. The points at the gap-rose contours mark the energies (the distances from the coordinate origin) where the electron spectra are suspected to have certain peculiarities. The latter should manifest themselves in the quasiparticle tunnel current-voltage characteristics (CVCs) (see Sec. V). The points belonging to the FS nd sections are marked as $\Delta$, and those belonging to the FS d sections as $D$. The subscript denotes the corresponding value of the momentum-space angular coordinate $\theta$. The point $\Delta_{45°} = 0$ was also included, because it participates in the formation of CVC peculiarities. Figures 2(c)–2(e) are arranged in such a way that the "complexity" of the corresponding electron spectrum increases. In particular, Fig. 2(d) corresponding to $N = 2$ contains an additional (in comparison to the case $N = 4$) peculiarity point $\Delta_{90°}$, which should make the overall CVC more complicated. The case $N = 2$ with large $\alpha > 45°$ [Fig. 2(e)] replaces the point $\Delta_{45°} = 0$ by the point $D_{45°} > 0$ and makes the gap to be nonzero over the whole FS. The shape of gap roses and hence the positions and even the existence of indicated points change with both the SCDW parameters ($\sigma_0$,$\alpha$,$N$) and the temperature $T$.

The area to the left of the solid curve in Fig. 2(a) corresponds to the states when CDWs are totally suppressed at $T = 0$ (i.e., the FS is not CDW gapped), and the SCDW becomes a dBCS ($\Delta = \Delta_0 = 1$, $\Sigma = 0$). But for points in the hatched section (between the solid and dotted curves), which are dBCS states at $T = 0$, the CDW order parameter $\Sigma$ arises at some finite temperature $T_r$ ($0 < T_r < T_s$), and the dBCS transforms into a genuine SCDW in the interval $T_r < T < T_s$. As an example, the parameter set ($N = 4$, $\Delta_0 = 1, \Sigma_0 = 0.9$, $\alpha = 20°$ [point D in Fig. 2(a)] was selected (the solid and dotted curves converge at $\alpha = 45°$, so that the temperature-driven CDW reentrance phenomenon disappears at $\alpha > 45°$, the latter values making sense only if $N = 2$). The corresponding $\Delta(T)$ and $\Sigma(T)$ dependencies are shown in Fig. 2(b), illustrating the temperature-induced CDW reentrance.

Specifically, at $T \leqslant T_r$, the CDW is suppressed, and we obtain a pure dBCS phase, with the corresponding gap rose of the parent dBCS (see Fig. 1); at $T_r < T \leqslant T_c$, the SCDW phase emerges, and the gap rose looks like that in Fig. 2(c); at $T_c < T < T_s$, a partially CDW-gapped normal metal exists with the corresponding gap rose (1); finally, at $T > T_s$, the CDWS becomes an ordinary metal. In Fig. 2(b), set D, the relationship $0 < T_r < T_c < T_s$ takes place. But a situation is also possible [83] when the whole $T$ interval with $\Sigma \neq 0$ is located below the superconducting critical temperature $T_c$, so that $0 < T_r < T_s < T_c$ [Fig. 2(b), set E]. All those transformations of the electron spectrum should manifest themselves in tunnel CVC as will be discussed below in more detail. Therefore, sets D and E are also included into the family of representative parameter sets.

The SCDWs to the left of the dotted curve in Fig. 2(a) are genuine dBCSs at any temperature below $T_c$.

Besides, in order to fully understand the mutual action of CDWs and superconductivity on CVCs, parallel calculations for either a dBCS or a nonsuperconducting CDW metal have to be done. But it cannot be either of the SCDW parents, because the actual $\Delta$ and $\Sigma$ values differ from their "bare" (parent) values rather substantially. In particular (see Fig. 2),

the magnitudes of $\Delta_0$ and $\Sigma_0$ (they are directly related to the strengths of corresponding pairing interactions) were selected to equal $\Delta_0 = \Sigma_0 = 1$ in each of Figs. 2(c)–2(e), but the actual zero-temperature $\Delta$ and $\Sigma$ deviate from unity. In this case, the comparison of relevant CVCs would be noninformative. Therefore, we selected a dBCS with the zero-$T$ superconducting gap equal to the actual one $\Delta(T = 0)$ for the corresponding SCDW. In order to distinguish from the representative order parameter set, we will refer to such a dBCSs and the corresponding CVCs as the related ones. The gap roses for such related dBCSs are shown in the corresponding panels by dashed curves. Note that, in Figs. 2(c) and 2(d), the gap roses for the SCDW and the related dBCSs coincide over a large part of their FS, including the nodal points. This circumstance allowed us to obtain the related CVCs that almost coincide with analyzed ones at least at low temperatures and low bias voltages (see below).

## III. DENSITY OF STATES

Before calculating tunnel CVCs, it is instructive to consider first the peculiarities in the electron DOSes, both differential and angle averaged, of SCDW. Fortunately, in the framework of the adopted SCDW model, the DOS can be obtained in the analytical form.

For simplicity, let us consider both CDW scenarios ($N = 4$ and 2) in detail only in the case $\alpha < 45^\circ$, which is appropriate to high-$T_c$ oxides. While calculating the electron DOS in the SCDW, it is expedient to use the polar coordinates $(\varepsilon,\theta)$ in the momentum space, where $\varepsilon > 0$ is the quasiparticle energy and $\theta$ is the angle reckoned from the axis $\mathbf{k}_x$. Then, the differential DOS $N(\varepsilon,\theta)$ can be written in the form,

$$N(\varepsilon,\theta) = N_F \,\mathrm{Re}\,\frac{\varepsilon}{\sqrt{\varepsilon^2 - \bar{D}^2(\theta)}}, \tag{16}$$

where $N_F$ is the density of states near the Fermi level in the parent (nongapped) metal, and $\bar{D}(\theta)$ is the gap profile given by Eq. (13). As usual [88],

$$N[\varepsilon < \bar{D}(\theta),\theta] = 0. \tag{17}$$

The angle-averaged dependence $N(\varepsilon)$ is given by the formula (the spectrum is two-dimensional),

$$N(\varepsilon) = \frac{1}{2\pi}\int_0^{2\pi} N(\varepsilon,\theta)\,d\theta. \tag{18}$$

For the sake of briefness, it is convenient to introduce the reduced DOS, $n(\varepsilon) = 2\pi N(\varepsilon)/N_F$.

### A. Checkerboard CDW

Let us first consider the SCDW with the checkerboard CDW ($N = 4$) in the general case with $\Delta \neq 0$ and $\Sigma \neq 0$. The corresponding gap rose is shown in Fig. 2(c). Its "Cartesian" representation (more precisely, the interval $0 \leqslant \theta \leqslant \pi/4$; it is enough for consideration, because the results are identical for other $\theta$ octants) is exhibited in Fig. 3, where all relevant points are marked; those are the energies where the DOS peculiarities can exist. From this figure, one can easily see that the DOS peculiarity positions are related to the gap-related

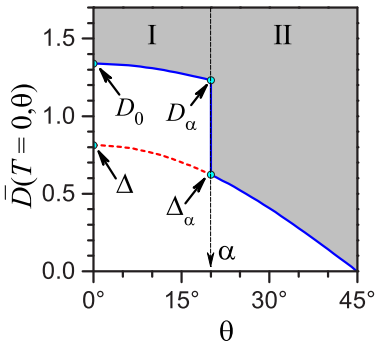


FIG. 3. (Color online) Cartesian representation of the gap rose shown in Fig. 2(c). $\bar{D}$ is the combined energy gap. Tinted regions I and II mark relevant intervals of integration over $\theta$ while calculating the electron density of states (DOS).

quantities $\Delta$, $\Sigma$, and $\alpha$ of the SCDW electrode by the formulas,

$$\Delta_\alpha = \Delta\cos 2\alpha, \tag{19a}$$

$$D_\alpha^2 = \Delta^2\cos^2 2\alpha + \Sigma^2, \tag{19b}$$

$$D_0^2 = \Delta^2 + \Sigma^2. \tag{19c}$$

Hence, the model parameters describing the SCDW state can be found from the positions of DOS peculiarities:

$$\Sigma = \sqrt{D_\alpha^2 - \Delta_\alpha^2}, \tag{20a}$$

$$\Delta = \sqrt{D_0^2 - D_\alpha^2 + \Delta_\alpha^2}, \tag{20b}$$

$$|\cos 2\alpha| = \Delta_a/\Delta. \tag{20c}$$

It is very remarkable that those relations remain valid for all temperatures. Another procedure [89] aimed at finding quasiparticle-spectrum parameters and explaining quasiparticle tunneling in layered-cuprate mesas should be pointed out.

According to condition (17), integration should be carried only in the tinted region. We should consider the intervals $0 < \theta < \alpha$ (I) and $\alpha < \theta < \frac{\pi}{4}$(II) separately. In the former, $\bar{D}^2(\theta) = \Sigma^2 + \Delta^2\cos^2 2\theta$, and the quantity,

$$\bar{n}_1(\varepsilon) = \mathrm{Re}\int_0^\alpha \frac{\varepsilon\,d\theta}{\sqrt{\varepsilon^2 - \Sigma^2 - \Delta^2\cos^2 2\theta}}, \tag{21}$$

has to be calculated. This is a tabulated integral [90], and, depending on $\varepsilon$, it equals

$$\bar{n}_1(\varepsilon \leqslant D_\alpha) = 0, \tag{22a}$$

$$\bar{n}_1(D_\alpha < \varepsilon \leqslant D_0) = \frac{\varepsilon''}{2}\left\{\mathbf{K}(\varepsilon') - F\left[\arcsin\left(\frac{1}{\varepsilon'}\cos 2\alpha\right),\varepsilon'\right]\right\}, \tag{22b}$$

$$\bar{n}_1(\varepsilon > D_0) = \frac{\varepsilon''}{2\varepsilon'}\left[\mathbf{K}\left(\frac{1}{\varepsilon'}\right) - F\left(\frac{\pi}{2} - 2\alpha, \frac{1}{\varepsilon'}\right)\right], \tag{22c}$$

where $\mathbf{K}(k)$ and $F(\varphi,k)$ are the complete and incomplete elliptic integrals of the first kind, respectively, and the notations $\varepsilon' = \sqrt{\varepsilon^2 - \Sigma^2}/\Delta$ and $\varepsilon'' = \varepsilon/\Delta$ were introduced to make the expressions shorter. It is easy to show that the dependence $n_1(\varepsilon)$ has a cusp at $\varepsilon = D_\alpha$ and a logarithmic singularity at $\varepsilon = D_0$.

In interval II, $\bar{D}(\theta) = \Delta\cos 2\theta$, and one needs to calculate

$$\bar{n}_{\rm II}(\varepsilon) = {\rm Re}\int_{\alpha}^{\pi/4} \frac{\varepsilon d\theta}{\sqrt{\varepsilon^2 - \Delta^2\cos^2 2\theta}}. \tag{23}$$

As a result,

$$\bar{n}_{\rm II}(\varepsilon \leqslant \Delta_\alpha) = \frac{\varepsilon''}{2}\mathbf{K}(\varepsilon''), \tag{24a}$$

$$\bar{n}_{\rm II}(\Delta_\alpha < \varepsilon \leqslant \Delta) = \frac{\varepsilon''}{2}F\left[\arcsin\left(\frac{1}{\varepsilon''}\cos 2\alpha\right), \varepsilon''\right], \tag{24b}$$

$$\bar{n}_{\rm II}(\varepsilon > \Delta) = \frac{1}{2}F\left(\frac{\pi}{2} - 2\alpha, \frac{1}{\varepsilon''}\right). \tag{24c}$$

Since $\Delta_\alpha \leqslant \Delta$, the peculiarity at $\varepsilon = \Delta_\alpha$ is a cusp. Besides, since we assume that $\alpha \neq 0^\circ$, branches (24b) and (24c) smoothly match at $\varepsilon = \Delta$, i.e., at $\varepsilon'' = 1$, and no additional CVC peculiarity arises.

The overall reduced DOS $n(\varepsilon)$ equals

$$n(\varepsilon) = 8[\bar{n}_{\rm I}(\varepsilon) + \bar{n}_{\rm II}(\varepsilon)], \tag{25}$$

where proper expressions have to be selected from Eqs. (22) and (24) for the components $\bar{n}_{\rm I}(\varepsilon)$ and $\bar{n}_{\rm II}(\varepsilon)$, respectively. The resulting DOS possesses cusps at $\varepsilon = \Delta_\alpha$ and $D_\alpha$, and a logarithmic singularity at $\varepsilon = D_0$. Among those energies, $\Delta_\alpha$ is always minimal, whereas $D_0$ is always maximal.

The formulas presented above do not depend explicitly on the temperature. The latter is hidden in the order parameters $\Delta \neq 0$ and $\Sigma \neq 0$, which are supposed to be known for any parameter set $(N, \Delta_0, \Sigma_0, \alpha, T)$. In particular, this circumstance means that, if a peculiarity survives at a certain temperature, it preserves its character (a cusp or a logarithmic singularity). However, the variation of any quantity from the indicated parameter set can result in the total suppression of either of order parameters and the corresponding modification of the electron spectrum, which will manifest itself in the changes of CVC profiles studied here. In the case $\Sigma = 0$ and $\Delta \neq 0$ (the pure dBCS), interval I is absent, and the DOS is described by formula (23) with $\alpha = 0$. Then, the whole spectrum is described by the expression [82],

$$n_{\rm dBCS}(\varepsilon) = 4 \times \begin{cases} \varepsilon''\mathbf{K}(\varepsilon'') & \text{for } \varepsilon < \Delta \\ \mathbf{K}\left(\frac{1}{\varepsilon''}\right) & \text{for } \varepsilon > \Delta \end{cases}, \tag{26}$$

with a single logarithmic singularity at $\varepsilon = \Delta$. In the case $\Sigma \neq 0$ and $\Delta = 0$ (the partially gapped metal), integrals (21) and (23) are trivial:

$$n_{\rm I}(\varepsilon) = \begin{cases} 0 & \text{for } \varepsilon < \Sigma \\ \frac{\alpha\varepsilon}{\sqrt{\varepsilon^2 - \Sigma^2}} & \text{for } \varepsilon > \Sigma \end{cases}, \tag{27}$$

$$n_{\rm II}(\varepsilon) = \frac{\pi}{4} - \alpha = \text{const}. \tag{28}$$

As a result [see formula (25)], we obtain a root singularity at $\varepsilon \to \Sigma + 0$. The latter statement may seem to contradict the statement made above that the singularity does not change its character with the parameter variation. However, here we obtain a situation when the singularity at $\varepsilon \to \Sigma + 0$ is formed not by an immediate vicinity of a single FS point characterized by the angle $\theta = 0^\circ$, but by all FS points within the angular sector $|\theta| \leqslant \alpha$.

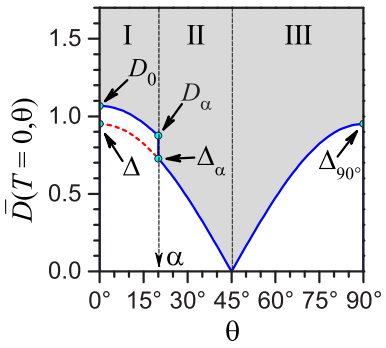


FIG. 4. (Color online) The same as in Fig. 3, but for the gap rose in Fig. 2(d).

### B. Unidirectional CDW

The case of unidirectional CDWs is a little bit more complicated. The "Cartesian" representation of the gap rose depicted in Fig. 2(d) and corresponding to the reference parameter set B and the temperature $T = 0$ is shown in Fig. 4. One can see that an additional peculiar point, $\Delta_{90^\circ}$, arises. The set of formulas (19) remains valid and becomes appended by one more equality,

$$\Delta = \Delta_{90^\circ}, \tag{29}$$

which is useful to check the consistency of the whole equation set. Attention should be paid to the fact that now the parameters $\Delta$ and $\Sigma$ must be determined for the unidirectional rather than the checkerboard CDW type.

Figure 4 demonstrates that, when calculating the DOS in the superconductor with unidirectional CDWs, it can be regarded as a combination of the DOSes for the checkerboard SCDW ($\theta$ intervals I and II in Fig. 4; cf. Fig. 3) and for the related dBCS ($\theta$ interval III in Fig. 4):

$$n(\varepsilon) = 4[\bar{n}_{\rm I}(\varepsilon) + \bar{n}_{\rm II}(\varepsilon) + \bar{n}_{\rm III}(\varepsilon)]. \tag{30}$$

Since $\Delta_{90^\circ} = \Delta$, Eq. (26) can be used to calculate $\bar{n}_{\rm III}(\varepsilon)$. Formulas (24) also remain the same for $\bar{n}_{\rm I}(\varepsilon)$ and $\bar{n}_{\rm II}(\varepsilon)$. As a result, the $n(\varepsilon)$ dependence has two cusps (at $\varepsilon = \Delta_\alpha$ and $D_\alpha$) and two logarithmic singularities (at $\varepsilon = \Delta$ and $D_0$).

The following remark distinguishing this case from the spectrum for set A should be made. The values of energies $\Delta_\alpha$ (the cusp) and $D_0$ (the logarithmic singularity) remain minimal and maximal, respectively. The other peculiarities, $\Delta_{90^\circ}$ (the logarithmic singularity) and $D_\alpha$ (the cusp), fall within the interval $(\Delta_\alpha, D_0)$, but their relative order can vary. The change in the peculiarity order can be induced by varying the SCDW parameters and/or the temperature. The condition that $\Delta_{90^\circ} = \Delta$ coincides with $D_\alpha$ can be easily obtained from Eq. (19b); it reads

$$\Delta\sin 2\alpha = \Sigma. \tag{31}$$

This relationship does not depend on the temperature explicitly as well. The $(\sigma_0, \alpha)$ pairs satisfying Eq. (31) at $T = 0$ are plotted on the $\sigma_0$-$\alpha$ phase diagram [Fig. 2(a)] as a dashed curve. Hence, for all SCDWs with parameter values located in the area between this curve and the dBCS boundary (the solid curve), e.g., for set B, the DOS peculiarity order at $T = 0$ is $\Delta_\alpha < D_\alpha < \Delta_{90^\circ} < D_0$, whereas for all parameter sets to the

right of the solid curve, e.g., for set C, one has $\Delta_\alpha < \Delta_{90^\circ} < D_\alpha < D_0$.

Finally, the extension of the CDW half-cone $\alpha$ beyond the limit of 45° gives rise to a complete FS gapping [see the gap rose in Fig. 2(e) plotted for parameter set C at $T = 0$]. In this case, the number of relevant peculiarities rises to five. Analytical expressions for $n(\varepsilon)$ can be derived in the same manner as was done above. Here, for brevity, only the contribution to the DOS of the new peculiarity $D_{45^\circ}$ is analyzed. Namely, we have to calculate the quantity,

$$n'(\varepsilon) \sim \mathrm{Re}\int_{\frac{1}{2}\arccos\frac{\sqrt{\varepsilon^2-\Sigma^2}}{\Delta}}^{\pi/4} \frac{\varepsilon d\theta}{\sqrt{\varepsilon^2-\Sigma^2-\Delta^2\cos^2 2\theta}} = \frac{\varepsilon}{\Delta}\mathbf{K}\left(\frac{\sqrt{\varepsilon^2-\Sigma^2}}{\Delta}\right). \quad (32)$$

Here, $n'$ means that we integrate only in the neighborhood of $\theta = \frac{\pi}{4}$. At $\varepsilon \to \Sigma + 0$, we obtain

$$n'(\varepsilon \to \Sigma + 0) = \frac{\pi\varepsilon}{\Delta},$$

and, at $\varepsilon < \Sigma$,

$$n'(\varepsilon < \Sigma) = 0.$$

Hence, there is a jump in the DOS at $\varepsilon = \Sigma$.

## IV. QUASIPARTICLE TUNNEL CURRENT ALONG $c$ AXIS

Tunneling is an essentially quantum-mechanical phenomenon, in which the idea of tunnel directionality is very important [91–93]. For instance, if it is neglected in calculations, the Josephson current in tunnel junctions with $d$-wave superconductors equals zero identically owing to its sensitivity to the order parameter sign. In principle, tunnel directionality has to be taken into consideration while calculating the quasiparticle tunnel current as well. However, in the case of the isotropic order parameter, the directionality effect results only in a reduction of the current magnitude, because all angle-dependent quantities can be factorized out and integrated independently, which gives rise to a simple renormalization of the junction resistance.

The effectiveness of tunnel directionality depends on whether tunneling is coherent or noncoherent. In this paper we consider either a tunnel junction between the $a$-$b$ crystal planes of two high-$T_c$ oxides, regarded as partially gapped $d$-wave SCDWs, so that the current is directed along the $c$-crystal axes of both electrodes (the symmetric setup) or a junction between a high-$T_c$ oxide and a normal metal (e.g., an STM tip, which means a nonsymmetric setup) with the current flowing also along the $c$ axis. Twist-crystal experiments of three kinds, namely, using bicrystals [94], the artificial cross-whiskers [95], and the natural cross-whiskers [96] show that the Josephson tunneling in this direction is incoherent, i.e., the tunneling is *not* restricted to that with coinciding quasiparticle momenta of linked states from both electrodes $\mathbf{k} = \mathbf{k}'$ [97]. For the Josephson current $I$, the observed nonzero values for the 45° twist [94–96], although smaller than expected for standard isotropic superconductors [88,98], testify that there should be at least an admixture of the $s$- or extended $s$-order parameter to the dominant $d$-wave one [97] (see our remark below). The observation of the nonstationary Josephson-effect terahertz radiation [99,100] also demonstrates the nodeless superconductivity in high-$T_c$ oxides. This fact contradicts the main body of coherent-tunnel experiments in the $a$-$b$ plane showing the $d$-wave character of superconductivity in high-$T_c$ cuprates [101–104]. At present, this controversy is far from being resolved. In the specific calculations carried out in this paper, we restrict the consideration to the $d$-wave case, which for the quasiparticle current gives the same results as if the extended $s$-wave order parameter [105] dominates so that our treatment is quite general. Of course, the study of the $c$-axis *Josephson current* needs a separate consideration for every symmetry.

On the other hand, the quasiparticle tunnel current $J$ being proportional to the functional of the product $G_1G_2$ [106], where $G_i$ symbolizes the normal Green's function of the $i$th $d$-wave SCDW electrode, is not averaged out for any degree of tunnel incoherence. The latter effect is inevitable for $I$, flowing between two $d$-wave SCDWs, because $I$ is the functional of the product $F_1F_2$ [106]. Here, $F_i$ is the anomalous Gor'kov Green's function for the $i$th $d$-wave SCDW electrode [107], and it is proportional to angular factor (8). Therefore, in our consideration of quasiparticle tunneling between SCDWs we chose the experimentally supported model of strongly incoherent tunneling.

The opposite case of the coherent tunneling would give similar results, so that our treatment is rather general and reproduces well peculiarities of $G(V)$ whatever the actual degree of tunneling coherence. Nevertheless, it might occur that the $c$-axis quasiparticle tunneling is governed by a mixture of coherent and incoherent transport although the degree of the mixture remains unknown [108].

The coherence versus noncoherence dichotomy in tunneling depends on the orientation of the velocity of tunneling charge carriers with respect to the normal $\mathbf{n}$ to the junction plane [97]. The predominately two-dimensional character of the SCDW spectrum allows the $k_z$-electron spectrum dispersion to be neglected while studying tunneling along the $c$ axis of a cuprate superconductor. When $c$ axes of both electrodes are parallel to $\mathbf{n}$, integration over the quasiparticle states in the momentum space can be carried out independently in the $a$-$b$ plane (the junction plane) and normally to it. Then, for the $c$-axis tunneling, there arises a situation similar to the isotropic pairing, when that or another model of the tunnel barrier can only change the effective tunnel resistance, keeping the functional behavior of $G(V)$ the same.

Bearing all the aforesaid in mind, the formulas for the quasiparticle tunnel current can be obtained in the conventional way [88,106], which was applied to the $s$-wave and $d$-wave SCDW cases and was described in more detail elsewhere [46,47,50,84,109,110]. In line with the previous treatments, the phenomenological tunnel-Hamiltonian approach was adopted [111]. All the properties of a barrier were incorporated into the single constant $R$ describing its normal-state resistance. The ultimate formula for the calculation of CVCs for the quasiparticle current through a tunnel junction created between the $a$-$b$ facets of two SCDWs looks like

$$J(V) = \frac{1}{2(2\pi)^2 eR}\int_{-\pi}^{\pi} d\theta \int_{-\pi}^{\pi} d\theta' \int_{-\infty}^{\infty} d\omega$$

$$\times K(\omega,V,T)P(\omega,\theta)P'(\omega-eV,\theta'). \quad (33)$$

Here,

$$K(\omega,V,T)=\tanh\frac{\omega}{2T}-\tanh\frac{\omega-eV}{2T}; \quad (34)$$

the limits of integration over $\theta$ and $\theta'$, as well as the absence of correlations between the latter, follows from the spectrum two dimensionality and the absence of tunnel directionality and coherence; and the $P$ factors describe SCDW electrodes. Primed quantities are associated with the electrode that the potential $V$ is applied to (the $V$ electrode); its counterelectrode will be referred to as 0 electrode. In particular, for the 0 electrode,

$$P(\omega,\theta)=\frac{\Theta(|\omega|-\bar{D}(T,\theta))}{\sqrt{\omega^2-\bar{D}^2(T,\theta)}}\times[|\omega|+\operatorname{sign}\omega\cos\varphi\,\bar{\Sigma}(T,\theta)], \quad (35)$$

where $\Theta(x)$ is the Heaviside step function, the CDW phase $\varphi$ is usually pinned by the junction interface and acquires the values 0 or $\pi$ (see discussion in Ref. [84]), and $\bar{D}(T,\theta)$ and $\bar{\Sigma}(T,\theta)$ are the gap and CDW-order-parameter profiles on the Fermi surface described by formulas (13) and (15), respectively. For $P'(\omega-eV,\theta')$, $\omega$ in formula (35) has to be changed to $\omega-eV$, and all other parameters but $T$ have to be primed, i.e., associated with the $V$ electrode. The second summand in the brackets in Eq. (35) represents the component related to the electron-hole-pairing Green's function $G_{ih}$, which is normal in the sense of being proportional to the product $c_l^\dagger c_r$ [112,113]. Here, subscripts $l$ and $r$ correspond to two different nested FS sections. On the other hand, it is "anomalous," because it includes the amplitude $\Sigma$ and phase $\varphi$ of the CDW order parameter in the same way the Gor'kov Green's function $F$ has a factor $\Delta$, i.e., a superconducting order parameter [88,106].

The ordinary expression for the quasiparticle current through a tunnel junction obtained in the framework of the tunnel Hamiltonian approach looks like [88,92]

$$J(V)=\frac{1}{2eR}\int_{-\infty}^{\infty}d\omega\,K(\omega,V,T)N(\omega)N'(\omega-eV), \quad (36)$$

where $N(\omega)$ and $N'(\omega)$ are the electron DOSes in the left- and right-hand side electrodes, respectively. Changing the order of integration in Eq. (33),

$$J(V)=\frac{1}{2eR}\int_{-\infty}^{\infty}d\omega\,K(\omega,V,T)\times\left\{\frac{1}{2\pi}\int_{-\pi}^{\pi}d\theta\,P(\omega,\theta)\frac{1}{2\pi}\int_{-\pi}^{\pi}d\theta'\,P'(\omega-eV,\theta')\right\}, \quad (37)$$

and introducing the quantity,

$$\tilde{N}(\varepsilon)=\frac{1}{2\pi}\int_{-\pi}^{\pi}d\theta\,P(\omega,\theta), \quad (38)$$

we can present $J(V)$ in the form similar to Eq. (36):

$$J(V)=\frac{1}{2eR}\int_{-\infty}^{\infty}d\omega\,K(\omega,V,T)\tilde{N}(\omega)\tilde{N}'(\omega-eV), \quad (39)$$

where (cf. formulas in Sec. III)

$$\tilde{N}(\varepsilon)=N(\varepsilon)+\delta N(\varepsilon) \quad (40)$$

is the DOS in the left-hand side electrode "modified" by the correction,

$$\delta N(\varepsilon)=\frac{\operatorname{sign}\varepsilon\cos\varphi}{2\pi}\operatorname{Re}\int_0^{2\pi}\frac{\bar{\Sigma}(T,\theta)\,d\theta}{\sqrt{\varepsilon^2-\bar{D}^2(T,\theta)}}, \quad (41)$$

to the electron-hole interaction, and $\tilde{N}'(\omega)$ is an analogous quantity for the right-hand side electrode. It looks like the electron-hole (CDW) pairing changes the role ("weight") of various electron states in tunneling. In particular, since $\bar{\Sigma}(T,\theta)\neq 0$ only within the $\theta$ interval I in Figs. 3 and 4 (the d FS sections), the modification concerns only the corresponding states $N_{\rm I}(\varepsilon)$. The correction term $\delta N(\varepsilon)$ can be calculated exactly if one pays attention that $\bar{\Sigma}(T,\theta)=\Sigma=\text{const}$ in this $\theta$ interval. As a result, we obtain

$$\delta N(\varepsilon)=\frac{\Sigma}{\varepsilon}\cos\varphi\,N_{\rm I}(\varepsilon), \quad (42)$$

where $\varepsilon$ can be of either sign.

## V. RESULTS AND DISCUSSION

Hence, in the framework of our model of tunneling through a junction with one or both SCDW electrodes, the calculations of the quasiparticle current were performed using formula (39). As a rule, the quasiparticle differential current-voltage characteristic, $G(V)=dJ/dV$, of the tunnel junction is much more informative than its original current-voltage characteristic $J(V)$. The CVC of a tunnel junction contains the combined and averaged information on the electron spectra in both electrodes. In particular, in the case of spatially homogeneous electrodes, the CVC peculiar points, which can be more or less pronounced, correspond to the sum of and, at $T\neq 0$, the difference between the peculiarity energies in the electron spectra of electrodes. In a good many cases, tunnel directionality can modify CVCs; for instance, if the electron spectrum is not isotropic, the resulting CVC depends on the orientation angles of electrodes with respect to the junction normal. At the same time, tunnel directionality cannot shift the positions of peculiar points.

The CVC shape is governed by the temperature $T$ and the intrinsic parameters of each electrode. In our case, these are the CDW sector half-width $\alpha$, the ratio $\sigma_0=\Sigma_0/\Delta_0$, which characterizes the relationship between the strengths of the parent electron-hole and Cooper pairings, and the type of CDWs, denoted by the number of the CDW sectors $N$. Depending on those parameters, the profiles of the overall energy gaps in the momentum space (gap roses) [8,83] change their forms and peculiarity locations. As a result, the CVC shape also changes.

We calculated the quasiparticle CVCs and studied their changes induced by varying the problem parameters in two representative cases: a junction between two identical SCDWs, which we will refer to as the symmetric one, and a junction between a SCDW and a normal metal interpreted as a special case of the SCDW (the nonsymmetric junction). The former is a model of the break junction, whereas the latter is typical of the

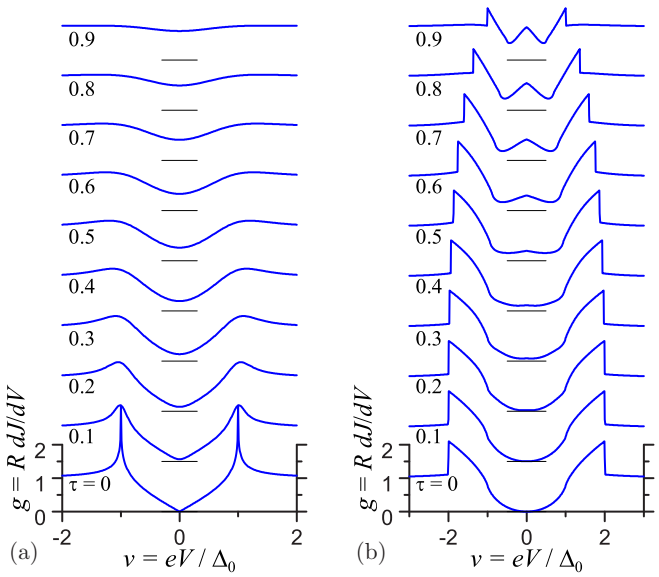


FIG. 5. (Color online) Temperature evolution of normalized quasiparticle conductance-voltage characteristics (CVCs) $g(v = \frac{eV}{\Delta_0}) = R\frac{dJ}{dV}$ for the $c$-axis quasiparticle tunnel current $J$ in nonsymmetric (a) and symmetric (b) tunnel junctions involving the dBCS electrode(s). Here, $e$ is the elementary charge, $V$ the bias voltage, and $R$ the junction resistance in the normal state.

STM. In both cases, the $c$ axis of the SCDW electrode (or both SCDW electrodes) is supposed to be oriented normally to the junction plane. Besides, the parameter $\cos\varphi$ in formula (35) was put equal to 1.

The dependencies of the dimensionless tunnel conductance $g = R\frac{dJ}{dV}$ on the dimensionless bias voltage $v = eV/\Delta_0$ were calculated by simulating the experimental procedure: namely, numerically, using the formula that can be reduced to the expression,

$$g(v) = R\frac{J(V+\delta V) - J(V-\delta V)}{2\delta V}. \tag{43}$$

This issue was discussed in more detail elsewhere [110]. In this work, the increment $\delta v$ of the dimensionless bias voltage for the numerical differentiation of the dependence $J(V)$ was selected to equal $\delta v = e\delta V/\Delta_0 = 0.001$.

Our choice of $\Delta_0$ as a normalizing factor for the energy quantities implicitly implies that superconductivity was selected to be a background against which CDWs develop. Therefore, it seems reasonable to have reference (in the conventional sense) CVCs for tunnel junctions, both nonsymmetric and symmetric, with the dBCS [82]. Then the influence of CDWs could be confidently singled out. The required sets of CVCs describing their temperature evolution are plotted in Fig. 5.

### A. Nonsymmetric junctions

The nonsymmetric configuration, i.e., the tunnel junction between an SCDW and a normal metal is much simpler for the analysis, because formula (33) is strongly simplified in this case. Really, a normal metal can be regarded as a limiting case of SCDW with no superconducting and CDW order parameters. Then, both $\bar{D}(T,\theta)$ and $\bar{\Sigma}(T,\theta)$ in formula (35) equal zero. As a result, the corresponding $\tilde{N}(\omega)$ dependence becomes identically equal to unity. It is convenient to select the primed electrode as a normal metal [$\tilde{N}' \equiv 1$ in Eq. (39)]. Then, the dependence of the tunnel current on the bias voltage $V$ is contained in kernel (34) only. Now, the formula for calculations looks like

$$J(V) = \frac{1}{2eR}\int_{-\infty}^{\infty} d\omega K(\omega,V,T)\tilde{N}(\omega). \tag{44}$$

Going further and putting also $\tilde{N}(\omega) \equiv 1$ in Eq. (44), i.e., assuming the unprimed electrode to be also a normal metal, we obtain an integral that gives the standard formula for the Ohmic contact, $J = V/R$.

In the case $T = 0$, formula (44), owing to the properties of the kernel $K(\omega,V,T)$, transforms into the expression,

$$J(V) = \frac{1}{eR}\int_0^{eV} d\omega\tilde{N}(\omega), \tag{45}$$

so that the conductance $G(V)$ equals

$$G(V) = \frac{dJ}{dV} = \frac{\tilde{N}(eV)}{R}. \tag{46}$$

Analytic expressions for the normalized components of $\tilde{N}(x)$ were obtained in Sec. III. They also allow one to give a qualitative interpretation to the influence of electron-hole pairing on the CVC form. In particular, if we put $\cos\varphi = 1$, formula (42) means that the CDWs enhance the role of states from the d FS sections in the formation of the positive CVC branch or compensate (or even overcompensate) the conventional term $N(\varepsilon)$ in the negative CVC branch. The correction is proportional to the ratio $\Sigma/|\varepsilon|$, so that the compensation should be the most effective at $\varepsilon = -\Sigma$. If $\cos\varphi = -1$, the enhancement/compensation situation will be inverse with respect to the voltage sign.

For $\cos\varphi = 0$, the tunnel CVCs would reveal their conventional, appropriate to the case of conventional superconductors, antisymmetry with respect to the voltage sign: $J(V) = -J(-V)$ [92]. As a consequence, the conductance $G(V) = dJ/dV$ becomes a symmetric function: $G(V) = G(-V)$. But as was shown earlier [45–47,114,115], any other value of $\varphi$ breaks this symmetry in the case of two different SCDW electrodes. Hence, in the framework of our approach, this circumstance (we recall that typical values of $\varphi$ are 0 and $\pi$, for which $\cos\varphi = \pm 1$) provides a natural explanation for the appearance of the dip-hump structures in only one voltage polarity branch of the cuprate tunnel spectra [89,116–118].

The availability of the correction term $\delta N(\varepsilon)$ in $\tilde{N}(\varepsilon)$ [see formula (40)] makes the whole CVC nonsymmetric and not proportional to the genuine DOS in the SCDW electrode spectrum. However, $N(\varepsilon)$ can be recovered from the CVC data. Indeed, in accordance with Eq. (42), the quantity $\delta N(\varepsilon)$ is asymmetric with respect to $\varepsilon$. This feature makes it possible to get rid of the anomalous contribution to $G(V)$ by symmetrizing the CVC, i.e., to evaluate the DOS using the formula,

$$N(E = eV) \sim \tfrac{1}{2}[G(V) + G(-V)]. \tag{47}$$

Now, let us consider the CVCs of the nonsymmetric junction for each representative SCDW parameter set.

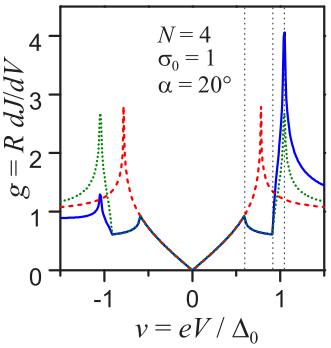


FIG. 6. (Color online) Normalized CVCs for tunnel junctions between the SCDW with the representative parameter set A (solid curve) or the related dBCS (dashed curve) and the normal electrode (the nonsymmetric junction) at $T = 0$. Vertical dotted lines mark the positions of CVC peculiarities $\Delta_a < D_\alpha < D_0$. For comparison, the corresponding DOS (in arbitrary units) is shown by the dotted curve.

#### 1. Set A: $N = 4, \sigma_0 = 1, \alpha = 20°$

In Fig. 6, the dimensionless conductance $g = RdJ/dV$ versus the dimensionless voltage $v = eV/\Delta_0$ is shown for the nonsymmetric junction between a normal electrode and a SCDW with parameter set A [see Fig. 2(a)], and at $T = 0$. The corresponding CVC for the related dBCS is also exhibited, as well as the DOS profile calculated by symmetrizing the CVC. One can see that, although the semiconductor model, which is valid for superconductors due to the drop out of the coherent factors from the formulas for the tunnel current [44], is also appropriate to the CDW case, the behavior of $G(V)$ for the SCDW differs from that for the dBCS. This is due to the existence of the "interband" Green's function, which describes the electron-hole pairing, and the corresponding term in the overall quasiparticle tunnel current [45,119]. As a result, the function $G(V)$ is highly nonsymmetric and possesses three (besides the obvious peculiarity located at $V = 0$) features directly connected to the peculiarity points in Fig. 2(c), as was discussed in Sec. III.

Let us first consider the CVC changes induced by separately varying $\sigma_0$ and $\alpha$ parameters. The corresponding illustrations are shown in Fig. 7. The lowest CVCs in both panels are completely symmetric and identical. In the case of Fig. 7(a), the lowest CVC is associated with the parameter set D ($N = 4, \sigma_0 = 0.9, \alpha = 20°$), which, as was discussed in Sec. II, corresponds at $T = 0$ to the state of pure dBCS [see Fig. 2(b)]. The parameter set for the lowest CVC in Fig. 7(b) also corresponds to the pure dBCS because the d FS sections are absent ($\alpha = 0°$). Going over the CVCs upwards in both panels, we increase the order parameter $\Sigma$, which makes the CVCs more and more nonsymmetric. In particular, the $\Sigma$ value for the set ($N = 4, \sigma_0 = 1, \alpha = 5°$)—this is the next CVC in Fig. 7(b)—is too small for some distortions of the peaks to be observed at the selected scale; however, the difference between the peak heights can already be detected. This is a result of the detrimental effect of the electron-hole pairing on the superconducting one. Changing to larger $\sigma_0$ or $\alpha$, we enhance the role of the former pairing, so that $\Sigma$ tends to its parent value $\Sigma_0$, and hamper the latter pairing, so that $\Delta \to 0$. As a result, the peculiarities associated with $\Delta$ only [these

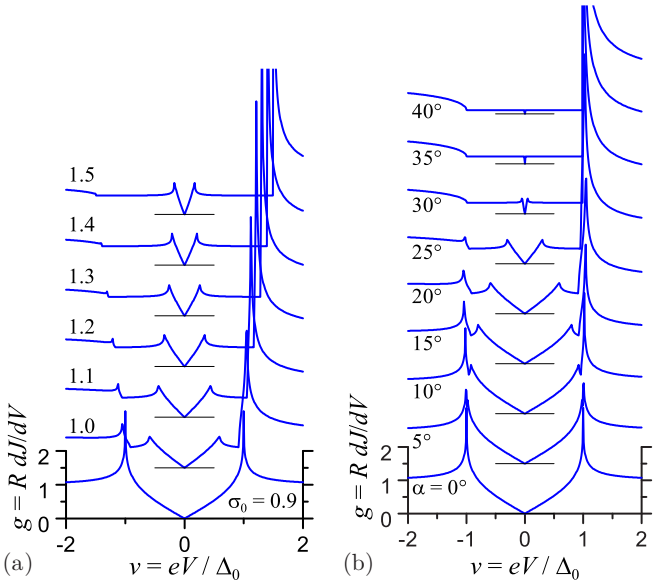


FIG. 7. (Color online) Modifications of the CVC for the nonsymmetric junction with SCDW parameter set A induced by changing (a) parameter $\sigma_0$ and (b) parameter $\alpha$, at $T = 0$.

are $\pm\Delta_\alpha$; see Figs. 2(c) and 6], decrease by magnitude and move towards $V = 0$. The other peculiarities (these are $\pm D_\alpha$ and $\pm D_0$) tend to $\pm\Sigma$, which in turn tend to $\pm\Sigma_0$. However, as was said above, if $\cos\varphi = 1$, all $\Sigma$-related singularities become effectively compensated in the vicinity of $eV = -\Sigma$ (these are $-D_\alpha$ and $-D_0$), in contrast to the behavior of the $D_\alpha$ and $D_0$ peculiarities in the positive $V$ branch.

Both panels clearly illustrate how doping-induced changes of problem parameters can affect the CVCs of nonsymmetric junctions. Such modifications should be observed, e.g., in STM measurements. The manifestations of relevant peculiarities may be substantially reduced by the disorder. The latter should significantly influence the parameters $\alpha$ and $\sigma_0$. This complication is unavoidable, especially for such nonstoichiometric compounds as cuprates [120–122], which may give rise to an appreciable smearing of CVC peculiarities.

Not only the spatial inhomogeneity can hamper the observation of CVC peculiarities. In Fig. 8(a), the temperature evolution of CVCs is depicted for a nonsymmetric junction involving the SCDW with representative parameter set A. Figure 8(b) demonstrates the temperature-driven evolution of the CVC feature points. The most pronounced effect is the strong smearing of all peculiarities. It happens because, according to Eq. (44), when calculating $dJ/dV$, we actually average $\tilde{N}(\omega)$ over a certain $\omega$ interval, the width of which grows as the temperature increases. Therefore, any cusps and logarithmic singularities, which are integrable *per se*, are smoothed out at $T \to T_c$. However, their behavior in both $V$ branches is different. In particular, as follows from Fig. 2(b), $\Sigma$ increases and $\Delta$ decreases as the temperature grows up to $T_c$. Hence, the $\pm\Delta_\alpha$ peculiarities are smoothed out by both $T$ and the reduction of $\Delta$. Again, the behavior of the peculiarities $\pm D_\alpha$ and $\pm D_0$ strongly depends on the branch polarity. Despite the increase of $\Sigma$ at $T \to T_c$, the convergence of the $-D_\alpha$ and $-D_0$ peculiarities to $-\Sigma$ results in their

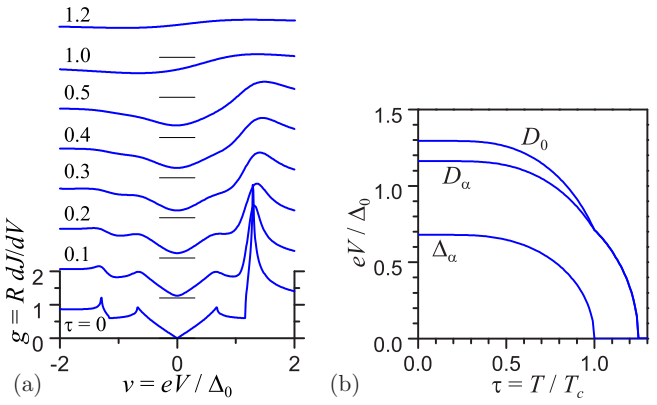


FIG. 8. (Color online) Temperature evolution of (a) CVCs for the nonsymmetric junction with SCDW parameter set A and (b) the corresponding CVC peculiarities.

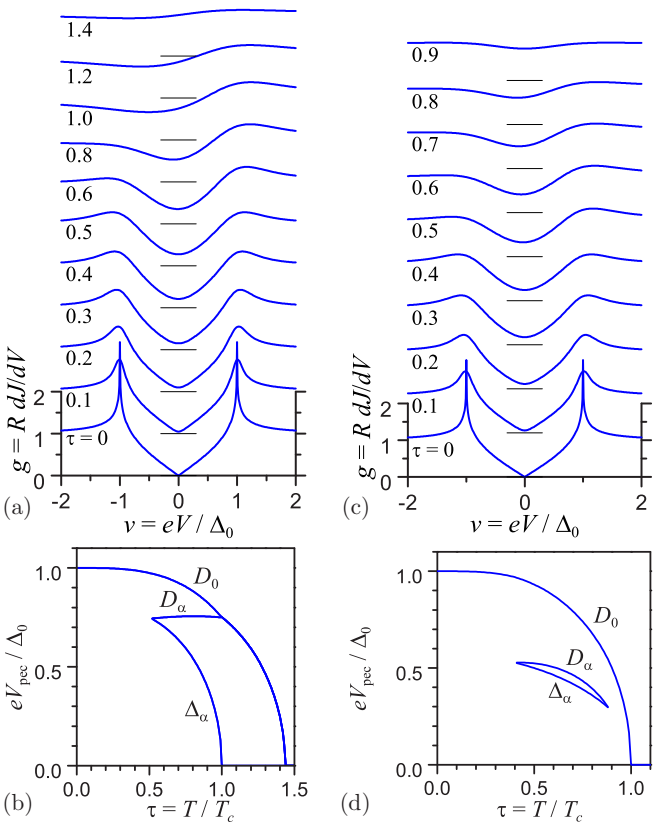


FIG. 9. (Color online) Temperature evolution of CVCs (a) and (c), and the corresponding CVC peculiarities (b) and (d) for the nonsymmetric junctions with SCDW parameter sets D (a) and (b) and E (c) and (d).

effective disappearance, whereas the $D_\alpha$ and $D_0$ peculiarities survive and strengthen, giving the CVC a form that strongly resembles the pseudogap phenomenon observed in cuprates.

By comparing the figures presented in this section and Fig. 5(a), one can see that the CDW-induced pseudogapping of the electron spectrum totally distorts the CVCs of the parent $d$-wave superconductor, making it more complicated and asymmetric within the whole $T$ interval of CDW existence, including $T = 0$. As will be demonstrated below, this conclusion remains valid for all examined representative cases, including symmetric junctions as well [see Fig. 5(b)]. Of course, a strong enough CDW disorder can severely reduce the CDW effects. This issue goes beyond the scope of this work. However, we believe that such pronounced effects as extra CVC peculiarities and CVC asymmetry will not completely disappear and could be unequivocally detected, at least for SCDW samples with a low CDW disorder.

#### 2. *Sets D and E: CDW reentrance*

Figure 2 shows that, by changing the parameter $\sigma_0$ of the representative parameter set A to a value of 0.9, i.e., transforming it to parameter set D, we obtain a pure dBCS phase at $T = 0$ [83], so that the corresponding CVC turns out symmetric [Fig. 7(a)]. It is clear that switching on CDWs in the framework of our phenomenological approach means an increase of $\sigma_0$ and/or $\alpha$. Then, the CVCs will remain symmetric up to a certain value of the variable parameter and thereafter will be nonsymmetric.

Figure 2(b) testifies that, for parameter set D, the temperature can also be used to switch CDWs on. The corresponding evolution of the CVCs and the temperature dependencies of peculiarity point values are depicted in Fig. 9. Figure 9(b) demonstrates that the CVC peculiarities $\Delta_\alpha$ and $D_\alpha$ appear only above a certain temperature $T_r$. In the CVCs, they are strongly smeared and probably are not observable. At the same time, their appearance correlates with the appearance of CVC nonsymmetricity.

The temperature evolution of CVCs and CVC peculiarities in the case of CDWs almost suppressed by superconductivity [Fig. 2(b), set E] are shown in Figs. 9(c) and 9(d), respectively. Here, weak $\Sigma$-induced features emerge at $T_r$ and disappear at $T_s$ against the dominating superconducting background. As $T$ grows, the conventional CVC symmetry becomes broken when crossing this region and restored after leaving it.

Attention should be attracted to the fact that the CVCs at various $T$'s might be interpreted as a result of spectrum gapping by a single order parameter. This parameter seems to be almost temperature independent up to the critical temperature (in our case, this is $T_s$). Up to a certain $T_c < T_s$, the sample is a superconductor. Within this interval ($T < T_c$), something happens, so that the sample remains to be a superconductor, but the CVC for its tunnel junction with a normal metal loses its symmetric character and gradually takes a form inherent to the pseudogapped one. However, this interpretation is wrong. Actually, there are two intertwining order parameters.

#### 3. *Set B: $N = 2, \sigma_0 = 1, \alpha = 20°$*

For the unidirectional CDW pattern ($N = 2$), an additional feature point $\Delta_{90°}$ arises in the gap rose [Fig. 2(d)]. As was explained in Sec. III B, this peculiarity is responsible for the appearance of the logarithmic singularity in the DOS $N(\varepsilon)$ at $\varepsilon = \Delta$ and, as a consequence, two logarithmic CVC singularities at $eV = \pm\Delta$ (see Fig. 10).

Figure 11 illustrates the control of SCDW parameters $\sigma_0$ and $\alpha$ over the CVC. The interval of $\alpha$ in Fig. 11(b) was restricted

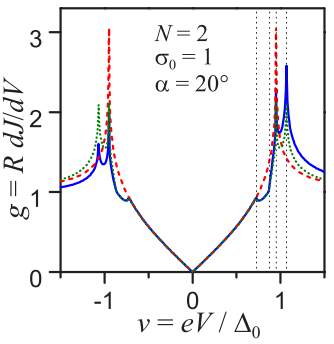


FIG. 10. (Color online) The same as in Fig. 6, but for SCDW parameter set B. Vertical dotted lines mark the positions of CVC peculiarities $\Delta_a < D_\alpha < \Delta_{90^\circ} < D_0$.

to $\alpha \leqslant 45^\circ$, because at larger $\alpha$'s the gap rose transforms into the form depicted in Fig. 2(e).

The $T$-induced variations of the CVC for the nonsymmetric junction involving a SCDW with parameter set B are shown in Fig. 12(a), and the temperature evolution of all four CVC peculiarities is demonstrated in Fig. 12(b). In Sec. III B, it was shown that at $T = 0$, the CVC peculiarity $\Delta_{90^\circ}$ can be located in either of the intervals $[\Delta_\alpha, D_\alpha]$ or $[D_\alpha, D_0]$ depending on the specific parameter set. From Fig. 12(b), it is evident that in the latter case the plots of the dependencies $\Delta_{90^\circ}(T)$ and $D_\alpha(T)$ have to intersect each other at a certain temperature $T$, and the CVC peculiarities change their relative order.

The approach of the parameter $\sigma_0$ to 0.9 would also bring us to the situation with the CDW reentrance. We will not analyze this case in detail. It is enough to mention that all characteristic temperatures remain the same, and the $\Delta$ and $\Sigma$ values vary in the range of their coexistence similarly to their behavior for the checkerboard CDW geometry [83]. Therefore, all corresponding CVC dependencies on the SCDW parameters and the temperature are analogous to those depicted in Figs. 11 and 12.

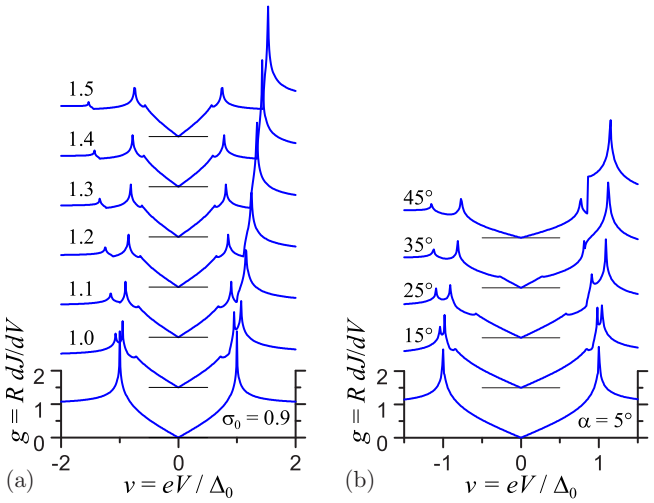


FIG. 11. (Color online) The same as in Fig. 7, but for SCDW parameter set B.

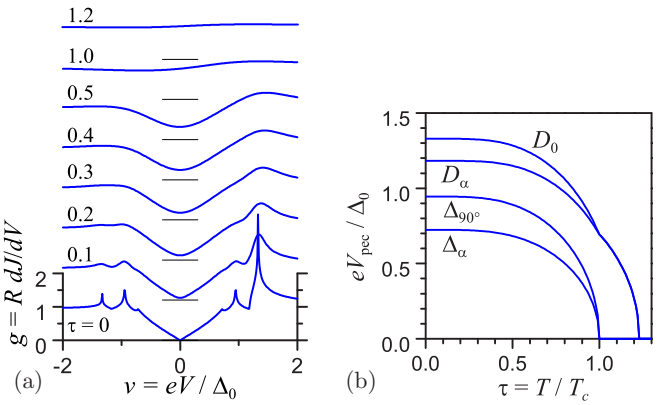


FIG. 12. (Color online) The same as in Fig. 8, but for SCDW parameter set B.

#### 4. *Set C:* $N = 2, \sigma_0 = 1, \alpha = 60^\circ$

In Fig. 13, the zero-temperature CVC for the representative SCDW with parameter set C is shown. Attention should be paid to a large jump in the positive branch and its absence in the negative one. This peculiarity at $D_{45^\circ}$ is a manifestation of the jump in the DOS at $\varepsilon = \Sigma$ [see the dotted curve and formula (32)]. Again, the corresponding electron-hole-pairing contribution enhances the peculiarity at $eV = D_{45^\circ}$ in the positive CVC branch (we recall that the CDW phase $\varphi = 0$) and compensates it in the negative one until its complete disappearance. Besides, possessing also a zero-conductance (full-gap) region at low bias voltages, the corresponding CVC drastically differs from that for the related dBCS.

Figure 14 illustrates the dependencies of the corresponding nonsymmetric CVCs on $\sigma_0$ and $\alpha$. Figure 14(b) is, in some sense, a continuation of Fig. 11(b). At the same time, as the phase diagram shows [Fig. 2(a)], the parameter $\sigma_0$ can be extended down to much smaller values without entering the dBCS region.

In Fig. 15, the temperature evolution of the CVC and the peculiarity energies are shown.

Summarizing the results of calculations obtained for nonsymmetric junctions, we may state that, for homogeneous electrode specimens, the CVCs measurements would allow one to find the SCDW parameters in rather a straightforward

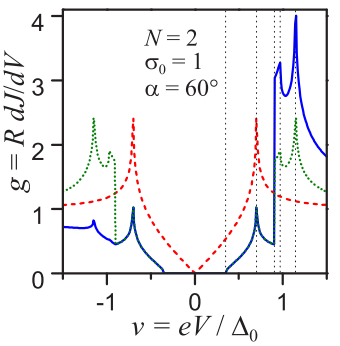


FIG. 13. (Color online) The same as in Fig. 6, but for SCDW parameter set C. Vertical dotted lines mark the positions of CVC peculiarities $\Delta_a < \Delta_{90^\circ} < D_{45^\circ} < D_\alpha < D_0$.

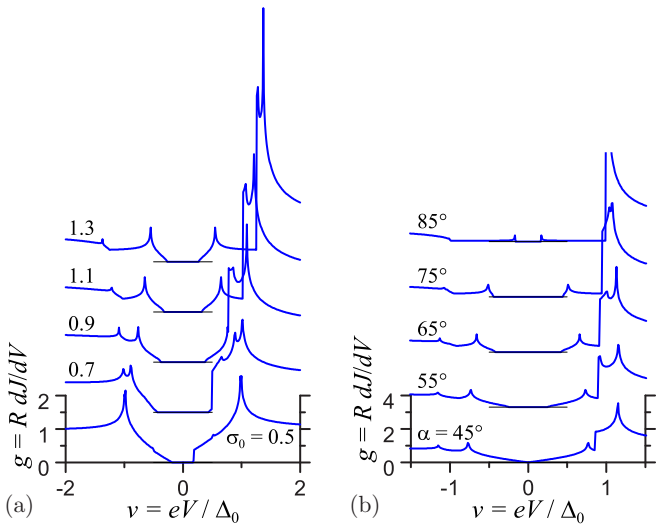


FIG. 14. (Color online) The same as in Fig. 7, but for SCDW parameter set C.

manner but only at low $T$. However, both an intrinsic inhomogeneity and finite temperatures will inevitably smear useful information concerning peak locations. Anyway, the obtained CVCs agree rather well with main experimental features. In particular, all of them demonstrate a pseudogap behavior at high temperatures, which we associate with the CDW gapping.

### B. Symmetric junctions

To calculate CVCs for the symmetric tunnel junction between two identical SCDWs, we have to put the corresponding parameters in both electrodes identical, so that

$$\tilde{N}(\omega) = \tilde{N}'(\omega), \tag{48}$$

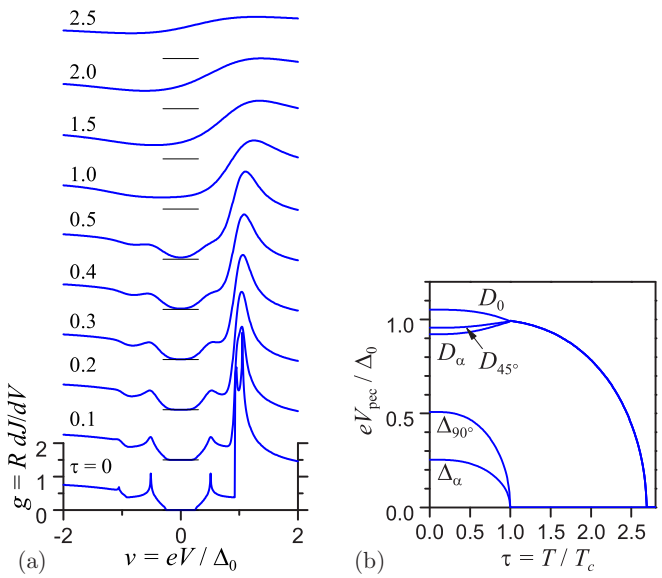


FIG. 15. (Color online) The same as in Fig. 8, but for SCDW parameter set C.

in Eq. (39). As a result, the terms linear in $\Sigma$ mutually compensate each other in both $V$ branches. Only the term quadratic in $\Sigma$ survives, so that the expression for the current becomes insensitive to the $\Sigma$ sign and antisymmetric with respect to the change of the bias voltage polarity.

The number of CVC peculiarities considerably increases. In particular, if the number of different nonzero peculiarities ($\varepsilon_{\mathrm{pec}i} \neq \varepsilon_{\mathrm{pec}\,j}$ if $i \neq j$) in the DOS spectrum with a node point $\Delta_{45°} = 0$ [see Figs. 2(b) and 2(c)] equals $S$, the CVC peculiarities in each branch will include the following ones. At $T \geqslant 0$ (the primed quantities are related to the right electrode),

(i.) $S$ peculiarities of the type $\Delta_{45°} + \varepsilon'_{\mathrm{pec}i} = \varepsilon_{\mathrm{pec}i} + \Delta'_{45°}$,

(ii.) $S$ peculiarities of the type $\varepsilon_{\mathrm{pec}i} + \varepsilon'_{\mathrm{pec}i} = 2\varepsilon_{\mathrm{pec}i}$, and

(iii.) $S(S-1)/2$ peculiarities of the type $\varepsilon_{\mathrm{pec}i} + \varepsilon'_{\mathrm{pec}\,j}$ ($i \neq j$).

At $T > 0$, additional peculiarities arise:

(iv) $S(S-1)/2$ peculiarities of the type $|\varepsilon_{\mathrm{pec}i} - \varepsilon'_{\mathrm{pec}\,j}|$ ($i \neq j$) and

(v) a combined peculiarity at $eV = 0$ of the type $|\varepsilon_{\mathrm{pec}i} - \varepsilon'_{\mathrm{pec}i}|$ formed by all DOS peculiarities.

Hence, the number of CVC peculiarities equals $S(S+3)/2$ at $T = 0$ and $S(S+1)+1$ at $T \neq 0$. Of course, each of the peculiarities can be more or less observable. But, because of their large number, we will not mark them explicitly, in contrast to what was done for nonsymmetric CVCs, since a cumbersome analysis is required in this case for the classification.

Let us consider symmetric CVCs for the representative parameter sets.

#### 1. *Set A:* $N = 4, \sigma_0 = 1, \alpha = 20°$

The dimensionless tunnel conductance $g(v)$ in the case of identical SCDW electrodes with parameter set A and at $T = 0$ is demonstrated in Fig. 16 (the solid curve), together with the $g(v)$ for the symmetric junction between the related dBCS electrodes (the dashed curve). One sees that the outer peak of the combined CDW-superconducting nature can be higher than its inner counterpart predominately formed by Cooper pairing. This is in agreement, e.g., with the tunnel measurements in underdoped $Bi_2Sr_2Ca_{1-x}Y_xCu_2O_{8+\delta}$ mesa structures [89]. Since the number of peculiarities in the spectrum of a SCDW with parameter set A equals three (except for the gap node $\Delta_{45°} = 0$), the number of CVC peculiarities in either of the CVC branches at $T = 0$ equals nine. As a result, the $g(V)$

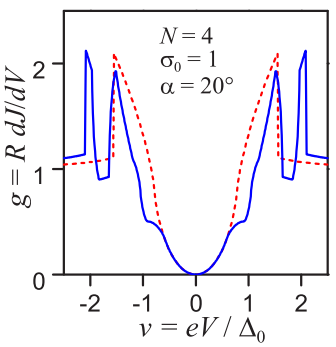


FIG. 16. (Color online) The same as in Fig. 6, but for the symmetric junction.

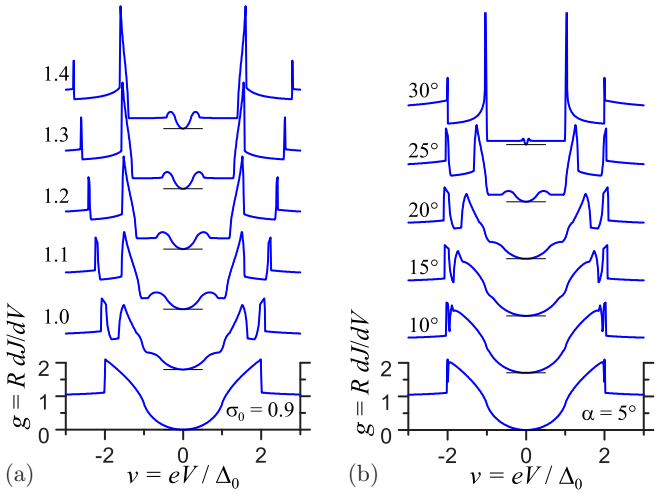


FIG. 17. (Color online) The same as in Fig. 7, but for the symmetric junction.

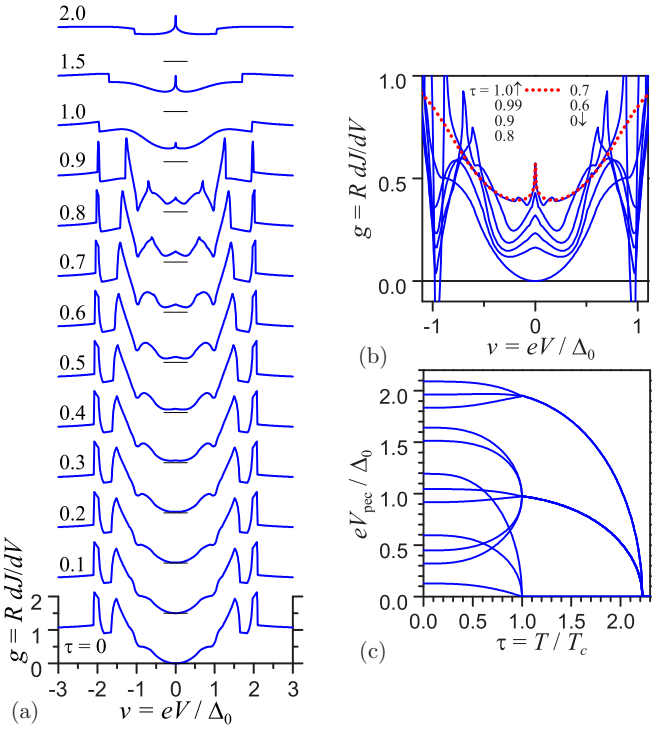


FIG. 18. (Color online) Temperature evolution of (a) CVCs for the symmetric junction with SCDW parameter set A and (c) the corresponding CVC peculiarities. (b) Scaled-up CVC sections near the zero-bias voltage.

plot differs strongly from the related CVC. The inner region of $g(V)$ also demonstrates the U behavior in the vicinity of $V = 0$. The deviation of $g(v)$ from the relative CVC starts (the appearance of a shoulder) at voltages, corresponding to the same point $\Delta_\alpha$ of the gap rose, as in the nonsymmetric case (Fig. 6).

Figure 17 makes it possible to trace the changes in the CVC induced by the variations of the intrinsic SCDW parameters $\sigma_0$ and $\alpha$. As a result, the forms of CVCs turn out to be rather diverse. The inner peak differs drastically from the single peak in the related CVC.

At the same time, the interplay between superconductivity and CDWs results in a rapid suppression of the "predominately superconducting" peaks. For intermediate $\alpha$'s, the peaks predominately related to the dielectric gap look very similar to superconducting ones and can be confused with them. A further increase of $\alpha$ totally suppresses superconductivity, and the results tend to those for normal metals partially gapped by CDWs [119].

The influence of $T$ makes the CVCs even more complicated. It is so because new points appear, equal to the differences between the spectrum peculiarities in the electrodes. Therefore, the total number of CVC peculiarities increases to 12 in either of the CVC branches. Besides, there emerges a peculiarity at $V = 0$ formed as an overlapping of gap-edge "self-differential" peculiarities produced by each of the spectral features [106]. The differential peculiarities are associated with the temperature-induced redistribution of quasiparticles over the energy levels outside the gapped region; they become more conspicuous as $T$ grows. It is clear that the "differential" peculiarities should be mainly located at low $V$'s.

The temperature evolution of peculiarities in the CVCs for symmetric junctions with SCDW [Fig. 18(a)] differs drastically from that in the non-symmetric-junction case [Fig. 8(a)]. First, the CVC peculiarities observed at $T = 0$ are not smeared by $T$, but remain well observable up to $T_c$. Second, the peculiarities arising at $T \neq 0$ are also not smeared, but even grow as $T \to T_c$. As a result, the CVCs become the most intricate near $T_c$. Figure 18(b) shows the behavior of $g(v)$ in the neighborhood of the actual superconducting temperature $T_c$. One can see a fine differential gap structure formed by both order parameters. The development and disappearance of the peculiarities is very intriguing and may be observed for break junctions made of "good enough" samples. This rich picture exists only below $T_c$, whereas the patterns above $T_c$ are more dull, exhibiting the pseudogap behavior particularly appropriate to cuprates [2,123,124].

This phenomenon has the following basis. In the symmetric case, every CVC peculiarity is a result of convolution of two DOS peculiarities (one from each electrode), which preserve their character (the cusp, jump or logarithmic singularity) within the whole temperature interval of their existence. It looks like the DOS peculiarities "support" each other, and the CVC peculiarity becomes "stronger" than the "strengths" of each "parent" DOS peculiarities, so that the kernel $K(\omega, V, T)$ in Eq. (36) cannot smooth it as much effectively as it does with a single DOS peculiarity in Eq. (44). In the particular case of isotropic BCS superconductor, such a phenomenon is also known. Namely, logarithmic singularities emerge in nonsymmetric junctions between different superconductors when the quasiparticle tunneling is carried out onto the levels with high DOSes above or below the energy gaps with merging edges [125].

The effect of CVC peculiarity "strengthening" becomes even stronger in the SCDW, because the electron-hole-pairing contribution to the overall effective DOS is linear in $\Sigma$, and $\Sigma$ is a growing function of $T$ up to $T_c$ [Fig. 2(b)]. By examining the behavior of various peculiarities in Fig. 18(a), we assert that the DOS peculiarities associated

with the d FS sections play the key role in all that: They "strengthen" each other ($\sim\Sigma^2$) and "support" the influence of the DOS peculiarities associated with the nd FS sections while convolution.

However, the temperature evolution of CVC is a gradual process, so that sooner or later the influence of $\Delta$ decrease at $T \to T_c$ has to prevail over that of $\Sigma$ growth. The results of calculations confirm this conclusion [Fig. 18(b)], but testify that the collapse of "extra" CVC peculiarities occurs in quite a narrow temperature interval near $T_c$.

Figure 18(c) demonstrates that in the course of evolution, the peculiarities can change their order, which makes the problem of their identification quite complicated.

For parameter set A, $T_s$ is substantially higher than $T_c$. Therefore, the predominantly $\Sigma$-driven peaks remain rather cute until $\tau = 1$. Above $\tau = 1$, only two peculiarities should remain in each CVC branch: at $|eV| = \Sigma(T)$ and $2\Sigma(T)$, as for a partially CDW-gapped normal metal [119]. This is really the case, as is seen from Fig. 18(a). However, the square-root singularity at $eV = \Sigma$ is substantially smeared for the actual parameters. The singularity at $eV = 2\Sigma$ is a jump, with its amplitude being gradually reduced by the thermal factor.

One should bear in mind that, under the influence of a sufficiently strong disorder-induced averaging in the inhomogeneous environment of nonstoichiometric cuprate samples [55–59], the whole spectral picture found above may be transformed into a V-like well with a dip-hump structure outside the superconducting gap edges [51].

### 2. *Sets D and E: CDW reentrance*

Similarly to what was done in the case of nonsymmetric junction (Fig. 9), the symmetric junctions with the reentrance parameter sets D and E will be analyzed. The relevant CVC temperature evolution is especially instructive (Figs. 19 and 20, respectively).

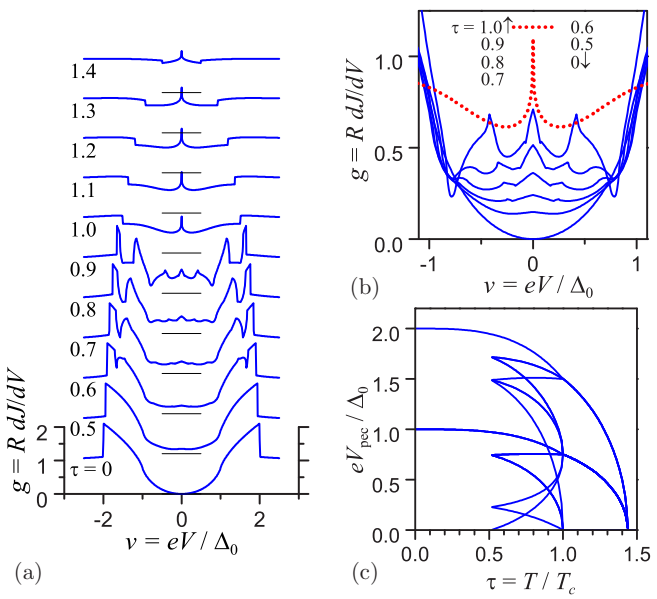


FIG. 19. (Color online) The same as in Fig. 18, but for SCDW parameter set D.

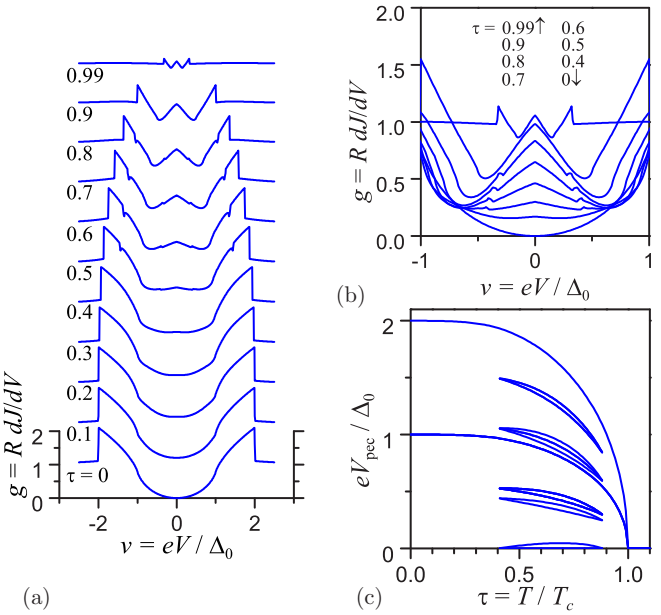


FIG. 20. (Color online) The same as in Fig. 18, but for SCDW parameter set E.

For set D, the appearance of the order parameter $\Sigma$ rapidly rising with $T$ conspicuously modifies $g(v)$, as stems from Fig. 19(a). The growth of (mostly $\Sigma$ determined) peculiarities with $T$ can be considered as a smoking gun of CDWs, since the $d$-wave superconducting features decrease with $T$. The pattern near $eV = 0$ [Fig. 19(b)] in the coexistence $T$ range is even more complicated than its counterpart for set A [Fig. 18(b)]. Here, according to Fig. 19(c), the peculiarity-position order also changes with $T$ as in Fig. 18(c).

When the CDW order parameter emerges and disappears below $T_c$ (set E), the temperature evolution demonstrates the same features as in case D (Fig. 19). However, since the $\Sigma$ magnitude is much smaller than in the previous case, these features are relatively weak. Besides, bearing in mind the detrimental influence of the inevitable dopant disorder and impurities [78], the phenomenon concerned can be easily overlooked.

### 3. *Set B: $N = 2, \sigma_0 = 1, \alpha = 20°$*

The conductances $g(v)$ describing tunneling at $T = 0$ between identical SCDW electrodes with parameter set B are demonstrated in Fig. 21. Since there are many different combinations of peculiar points in this case, the $g(v)$ plots exhibit a number of maxima and minima. The inner part of $g(v)$ remains incompletely gapped, showing the U behavior in the vicinity of $v = 0$. In this region, the CVC behavior is the same as in the related dBCS junction (the dashed curve). The only spread of the parent gap values here is caused by the trivial angular dependence (8) of the superconducting $d$-wave order parameter. However, the peculiarities in Fig. 21 are so close that the unavoidable disorder together with the less prominent thermal smearing should create wide joint peaks or broadened dip-hump patterns with two maxima and a trough between them. Such conductances were obtained for

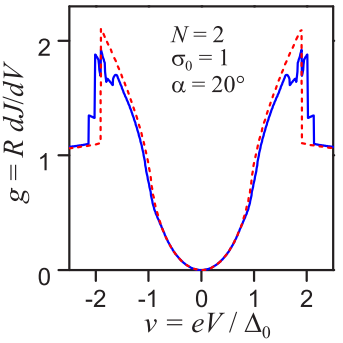


FIG. 21. (Color online) The same as in Fig. 16, but for SCDW parameter set B.

a number of cuprates in break-junction [49,116,118,126] and mesa [89,108,127–131] structures.

The conductances $g(v)$ strongly depend on the CDW parameters $\sigma_0$ and $\alpha$, as is shown in Fig. 22. This evolution can be studied by comparing the curves for differently doped samples.

The temperature evolution of $g(v)$ is shown in Fig. 23(a). Here, the pattern is very rich in singularities [cf. Fig. 18(a)], which relatively slowly deform with $T$, so that, in principle, it is possible to resolve different peaks, at least at the helium temperature, using the break-junction technique [116] or by measuring intrinsic-tunneling CVCs in mesa structures [89]. The peak near $V = 0$ is weaker here than for the checkerboard CDWs, which is the consequence of only two CDW sectors influencing the conductance behavior.

The attribution of singular points to corresponding combinations of gaps can be found from Fig. 22(a). The highest peaks are observed at $|eV| = D_0 + \Delta_{90^\circ}$, whereas at the largest relevant peculiar points $|eV| = D_0 + D_0 = 2D_0$ the peaks are as sharp as the highest ones, but much lower. A steep fall of $g(v)$ can be noticed at the differential points $|eV| = D_0 - \Delta_{90^\circ}$ [Fig. 22(a)], which of course can appear only at $T \neq 0$. The fine structure [132] in the break-junction tunnel spectra of $Bi_2Sr_2CaCuO_{8+\delta}$ observed at $T = 4.2K$ and becoming stronger at higher $T$ is similar to our theoretical results presented in Fig. 22 and might be interpreted as the intertwining between $d$-wave superconductivity and uniaxial CDWs. If such an interpretation is true, the outer gap features should be associated with the combined gap rather than the pure superconducting one in agreement with the experiment for $Bi_2Sr_2Ca_{1-x}Y_xCu_2O_{8+\delta}$ mesas [89]. Nevertheless, the original interpretation [132] of the observed conspicuous subgap structure as the influence of nonequilibrium phonons cannot be ruled out. In this connection, it would be useful to carry out measurements for a number of samples from the same batch, but with varying charge-carrier concentrations and different CDW patterns.

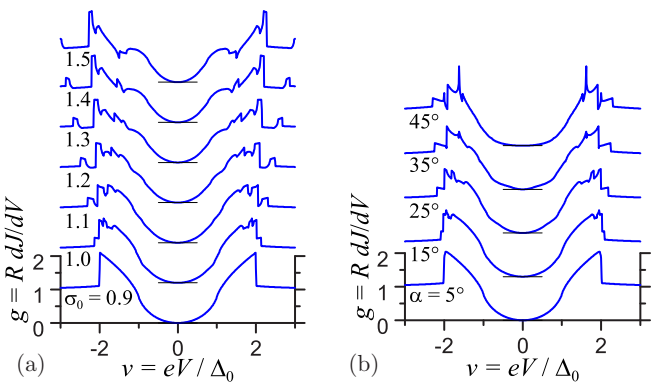


FIG. 22. (Color online) The same as in Fig. 17, but for SCDW parameter set B.

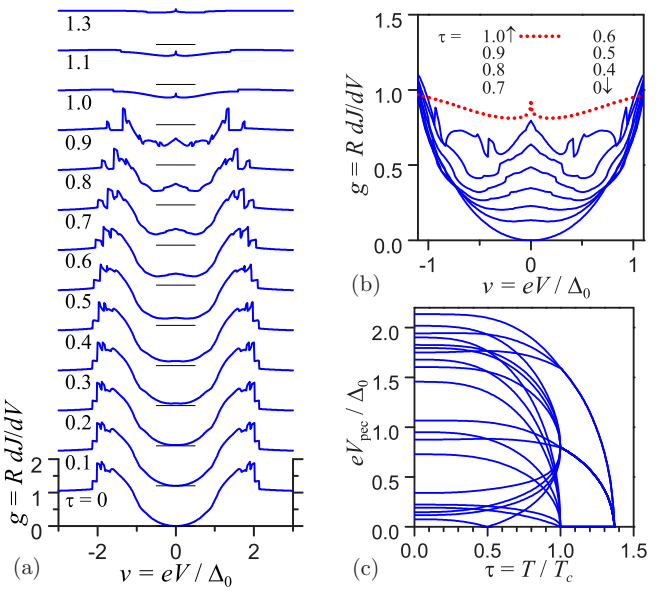


FIG. 23. (Color online) The same as in Fig. 18, but for SCDW parameter set B.

Interesting details of the tunnel spectrum $T$ evolution can be traced at small voltages, as is shown in Fig. 23(b), which is an excerpt from Fig. 23(a) in the neighborhood of the bias voltage origin. One sees that the fine structure develops with $T$, changes its form, and abruptly disappears at $\tau = 1$, the only remnant at $T > T_c$ being the logarithmic singularity at $eV = 0$ [119].

In Fig. 23(c), the temperature evolution of the peculiarity energies is displayed. It comes about that the relative locations of certain peculiarities change with $T$, so that their exact attribution would be difficult. The more so, the disorder may lead to their complete or partial merge.

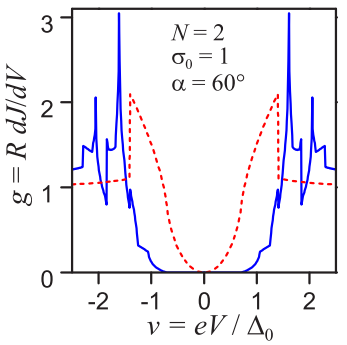


FIG. 24. (Color online) The same as in Fig. 16, but for SCDW parameter set C.

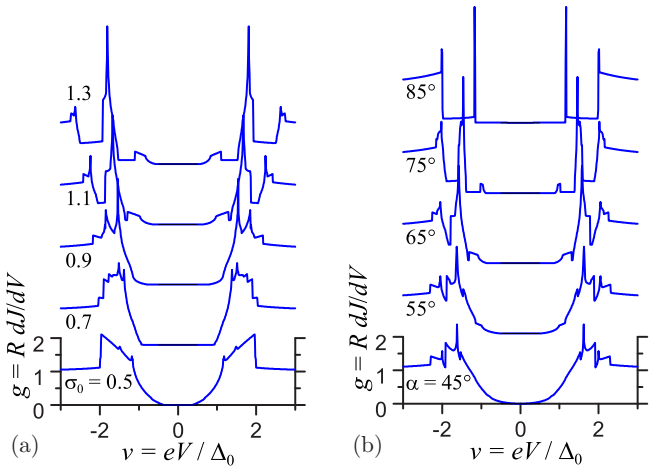


FIG. 25. (Color online) The same as in Fig. 17, but for SCDW parameter set C.

#### 4. *Set C:* $N = 2, \sigma_0 = 1, \alpha = 60°$

The conductances $g(v)$ for symmetric junctions with the SCDW (parameter set C) and the related dBCS, both at $T = 0$, are shown in Fig. 24. Contrary to case B, $g(v)$ is now fully gapped by both CDW and Cooper pairings. Even the huge peak in Fig. 24 is formed jointly by CDWs and $d$-wave superconductivity, similarly to the subtle features in the inner, fully gapped region. It might happen that the demonstrated here CDW-driven $s$-like gapping may mimic its superconducting counterpart and hide the effects of the nodes appropriate to the actual superconducting order parameter.

The obtained conductances $g(v)$ strongly evolve with the doping-related CDW parameters $\sigma_0$ and $\alpha$, as is displayed in Figs. 25(a) and 25(b), respectively. The inner region remains more or less structureless during the evolution.

On the other hand, temperature makes a more profound effect, in particular, filling the gap and introducing a complicated pattern near $eV = 0$ [see Fig. 26(a)]. The excerpt from Fig. 26(a) is depicted in Fig. 26(b) at a larger scale. It is quite different from the CVC for parameter set B shown in Fig. 23(b). The CVC $T$ evolution in the vicinity of $eV = 0$ demonstrated in Fig. 26(b) shows the intersection of peculiarities. Hence, the pattern changes qualitatively and not regularly. The intersection itself becomes clear from Fig. 26(c), where dependencies of peculiarities are shown in the whole temperature region up to the CDW critical temperature $T_s$.

## VI. CONCLUSIONS

Our calculations showed that the incoherent $c$-axis tunneling in cuprates studied by STM (STS), break-junction technique or intrinsic transport in mesas can reveal interesting joint electron spectrum gapping with manifestations of both $d$-wave superconducting and CDW features. Checkerboard and uniaxial CDWs were considered and demonstrated different tunnel conductance $G(V)$ patterns. The results *cannot be reduced* to a superposition of two kinds of gapping. Specifically, there is quite a number of peculiar points in the two-dimensional gap rose (angular diagram) in the momentum space. All of them are reflected in the tunnel conductance

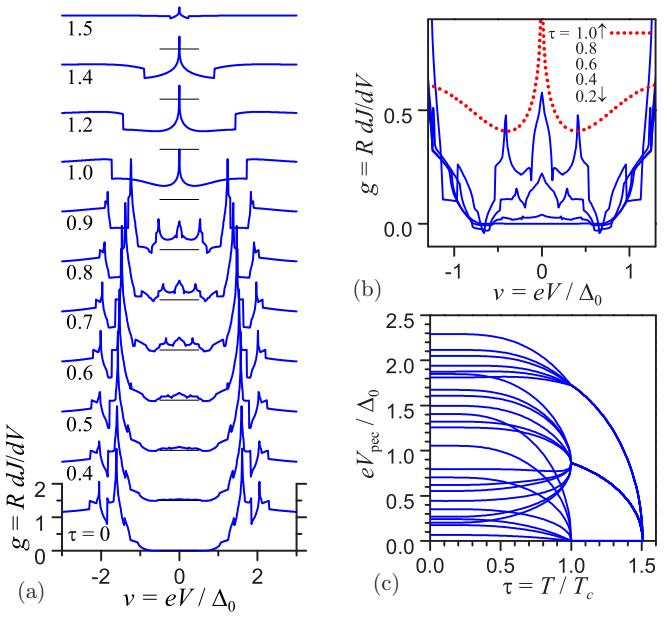


FIG. 26. (Color online) The same as in Fig. 18, but for SCDW parameter set C.

$G(V)$ in the nonsymmetric setup when one electrode is a normal metal and another one is an SCDW. In the case of two SCDW electrodes extra peculiarities appear in $G(V)$ due to the possibility of various combinations between the gap-rose singularities, which give their contributions to the current. The fine structure of $G(V)$ was shown to be strongly smeared by thermal broadening in the case of nonsymmetric setup. At the same time, unexpectedly, it turned out rather robust for symmetric tunnel junctions, which makes them preferable in tunnel researches. Of course, additional blurring will be induced by the inhomogeneities intrinsic to berthollides, including high-$T_c$ oxides [55–59]. However, their remnants may be seen in experimental data as wide complicated structures both inside and outside the superconducting-gap region. Such structures have been found and extensively studied, in particular, in $Bi_2Sr_2CaCuO_{8+\delta}$ [132]. The well-known dip-hump pattern observed in various cuprate CVCs both in the superconducting and normal state (above $T_c$) [89,116–118,127] seems to be a particular case of the general behavior when the disorder smears the CVC forcing different peculiarities to merge. Careful analysis of CVCs may not only reveal CDWs but also distinguish between uniaxial and checkerboard structures. In the case of symmetric junctions it would be of benefit to carry out such an analysis together with studying stationary Josephson current dependence on doping and temperature as was done in the case of intrinsic tunneling in $Bi_2Sr_2Ca_{1-x}Y_xCu_2O_{8+\delta}$ mesas [89].

## ACKNOWLEDGMENTS

The work was partially supported by Project No. 24 of the Scientific Cooperation Agreement between the Polish Academy of Sciences and the National Academy of Sciences of Ukraine for 2015–2017. Discussions with Alexander Kordyuk (Institute of Metal Physics, Kyiv) were very helpful.

[1] B. Keimer, in *Emergent Phenomena in Correlated Matter Modeling and Simulation*, edited by E. Pavarini, E. Koch, and U. Schollwöck, Vol. 3 (Forschungszentrum Jülich, Jülich, 2013), p. 9.1.

[2] M. Hashimoto, I. M. Vishik, R.-H. He, T. P. Devereaux, and Z.-X. Shen, Nature Phys. **10**, 483 (2014).

[3] M. Le Tacon, A. Bosak, S. M. Souliou, G. Dellea, T. Loew, R. Heid, K.-P. Bohnen, G. Ghiringhelli, M. Krisch, and B. Keimer, Nature Phys. **10**, 52 (2014).

[4] A. J. Achkar, X. Mao, C. McMahon, R. Sutarto, F. He, R. Liang, D. A. Bonn, W. N. Hardy, and D. G. Hawthorn, Phys. Rev. Lett. **113**, 107002 (2014).

[5] D. G. Hawthorn and A. J. Achkar, Phys. Canada **70**, 13 (2014).

[6] A. Kaminski, T. Kondo, T. Takeuchi, and G. Gu, Phil. Mag. **95**, 453 (2015).

[7] A. M. Gabovich, A. I. Voitenko, T. Ekino, M. S. Li, H. Szymczak, and M. Pękała, Adv. Condens. Matter Phys. **2010**, 681070 (2010).

[8] T. Ekino, A. M. Gabovich, M. S. Li, M. Pękała, H. Szymczak, and A. I. Voitenko, Symmetry **3**, 699 (2011).

[9] S. E. Sebastian, N. Harrison, and G. G. Lonzarich, Rep. Prog. Phys. **75**, 102501 (2012).

[10] A. M. Gabovich and A. I. Voitenko, Fiz. Nizk. Temp. **39**, 301 (2013).

[11] W. Li, C. Zhang, X. Wang, J. Chakhalian, and M. Xiao, J. Magn. Magn. Materials **376**, 29 (2015).

[12] A. A. Kordyuk, Fiz. Nizk. Temp. **41**, 417 (2015).

[13] E. Fradkin, S. A. Kivelson, and J. M. Tranquada, Rev. Mod. Phys. **87**, 457 (2015).

[14] G. Ghiringhelli, M. Le Tacon, M. M. S. Blanco-Canosa, C. Mazzoli, N. B. Brookes, G. M. De Luca, A. Frano, D. G. Hawthorn, F. He, T. Loew, M. M. Sala, D. C. Peets, M. Salluzzo, E. Schierle, R. Sutarto, G. A. Sawatzky, E. Weschke, B. Keimer, and L. Braicovich, Science **337**, 821 (2012).

[15] A. J. Achkar, R. Sutarto, X. Mao, F. He, A. Frano, S. Blanco-Canosa, M. Le Tacon, G. Ghiringhelli, L. Braicovich, M. Minola, M. Moretti Sala, C. Mazzoli, R. Liang, D. A. Bonn, W. N. Hardy, B. Keimer, G. A. Sawatzky, and D. G. Hawthorn, Phys. Rev. Lett. **109**, 167001 (2012).

[16] J. Chang, E. Blackburn, A. T. Holmes, N. B. Christensen, J. Larsen, J. Mesot, R. Liang, D. A. Bonn, W. N. Hardy, A. Watenphul, M. v Zimmermann, E. M. Forgan, and S. M. Hayden, Nature Phys. **8**, 871 (2012).

[17] A. J. Achkar, F. He, R. Sutarto, J. Geck, H. Zhang, Y.-J. Kim, and D. G. Hawthorn, Phys. Rev. Lett. **110**, 017001 (2013).

[18] V. Thampy, M. P. M. Dean, N. B. Christensen, L. Steinke, Z. Islam, M. Oda, M. Ido, N. Momono, S. B. Wilkins, and J. P. Hill, Phys. Rev. B **90**, 100510 (2014).

[19] M. Hücker, N. B. Christensen, A. T. Holmes, E. Blackburn, E. M. Forgan, R. Liang, D. A. Bonn, W. N. Hardy, O. Gutowski, M. v. Zimmermann, S. M. Hayden, and J. Chang, Phys. Rev. B **90**, 054514 (2014).

[20] W. Tabis, Y. Li, M. Le Tacon, L. Braicovich, A. Kreyssig, M. Minola, G. Dellea, E. Weschke, M. J. Veit, M. Ramazanoglu, A. I. Goldman, T. Schmitt, G. Ghiringhelli, N. Barišić, M. K. Chan, C. J. Dorow, G. Yu, X. Zhao, B. Keimer, and M. Greven, Nat. Commun. **5**, 5875 (2014).

[21] T. P. Croft, C. Lester, M. S. Senn, A. Bombardi, and S. M. Hayden, Phys. Rev. B **89**, 224513 (2014).

[22] R. Comin, A. Frano, M. M. Yee, Y. Yoshida, H. Eisaki, E. Schierle, E. Weschke, R. Sutarto, F. He, A. Soumyanarayanan, Y. He, M. Le Tacon, I. S. Elfimov, J. E. Hoffman, G. A. Sawatzky, B. Keimer, and A. Damascelli, Science **343**, 390 (2014).

[23] E. H. da Silva Neto, P. Aynajian, A. Frano, R. Comin, E. Schierle, E. Weschke, A. Gyenis, J. Wen, J. Schneeloch, Z. Xu, S. Ono, G. Gu, M. Le Tacon, and A. Yazdani, Science **343**, 393 (2014).

[24] M. Först, A. Frano, S. Kaiser, R. Mankowsky, C. R. Hunt, J. J. Turner, G. L. Dakovski, M. P. Minitti, J. Robinson, T. Loew, M. Le Tacon, B. Keimer, J. P. Hill, A. Cavalleri, and S. S. Dhesi, Phys. Rev. B **90**, 184514 (2014).

[25] M. Bakr, S. M. Souliou, S. Blanco-Canosa, I. Zegkinoglou, H. Gretarsson, J. Strempfer, T. Loew, C. T. Lin, R. Liang, D. A. Bonn, W. N. Hardy, B. Keimer, and M. Le Tacon, Phys. Rev. B **88**, 214517 (2013).

[26] J. E. Hoffman, E. W. Hudson, K. M. Lang, V. Madhavan, H. Eisaki, S. Uchida, and J. C. Davis, Science **295**, 466 (2002).

[27] W. D. Wise, M. C. Boyer, K. Chatterjee, T. Kondo, T. Takeuchi, H. Ikuta, Y. Wang, and E. W. Hudson, Nature Phys. **4**, 696 (2008).

[28] Y. He, Y. Yin, M. Zech, A. Soumyanarayanan, M. M. Yee, T. Williams, M. C. Boyer, K. Chatterjee, W. D. Wise, I. Zeljkovic, T. Kondo, T. Takeuchi, H. Ikuta, P. Mistark, R. S. Markiewicz, A. Bansil, S. Sachdev, E. W. Hudson, and J. E. Hoffman, Science **344**, 608 (2014).

[29] T. Wu, H. Mayaffre, S. Krämer, M. Horvatić, C. Berthier, W. N. Hardy, R. Liang, D. A. Bonn, and M-H. Julien, Nature (London) **477**, 191 (2011).

[30] T. Wu, H. Mayaffre, S. Krämer, M. Horvatić, C. Berthier, P. L. Kuhns, A. P. Reyes, R. Liang, W. N. Hardy, D. A. Bonn, and M-H. Julien, Nat. Commun. **4**, 2113 (2013).

[31] T. Wu, H. Mayaffre, S. Krämer, M. Horvatić, C. Berthier, W. N. Hardy, R. Liang, D. A. Bonn, and M.-H. Julien, Nat. Commun. **6**, 6438 (2014).

[32] V. B. Zabolotnyy, A. A. Kordyuk, D. Evtushinsky, V. N. Strocov, L. Patthey, T. Schmitt, D. Haug, C. T. Lin, V. Hinkov, B. Keimer, B. Büchner, and S. V. Borisenko, Phys. Rev. B **85**, 064507 (2012).

[33] M. Hashimoto, E. A. Nowadnick, R.-H. He, I. M. Vishik, B. Moritz, Y. He, K. Tanaka, R. G. Moore, D. Lu, Y. Yoshida, M. Ishikado, T. Sasagawa, K. Fujita, S. Ishida, S. Uchida, H. Eisaki, Z. Hussain, T. P. Devereaux, and Z.-X. Shen, Nature Mater. **14**, 37 (2015).

[34] Y. Toda, F. Kawanokami, T. Kurosawa, M. Oda, I. Madan, T. Mertelj, V. V. Kabanov, and D. Mihailovic, Phys. Rev. B **90**, 094513 (2014).

[35] D. LeBoeuf, S. Krämer, W. N. Hardy, R. Liang, D. A. Bonn, and C. Proust, Nature Phys. **9**, 79 (2013).

[36] D. LeBoeuf, N. Doiron-Leyraud, J. Levallois, R. Daou, J.-B. Bonnemaison, N. E. Hussey, L. Balicas, B. J. Ramshaw, R. Liang, D. A. Bonn, W. N. Hardy, S. Adachi, C. Proust, and L. Taillefer, Nature (London) **450**, 533 (2007).

[37] N. Barišić, S. Badoux, M. K. Chan, C. Dorow, W. Tabis, B. Vignolle, G. Yu, J. Béard, X. Zhao, C. Proust, and M. Greven, Nature Phys. **9**, 761 (2013).

[38] E. H. da Silva Neto, R. Comin, F. He, R. Sutarto, Y. Jiang, R. L. Greene, G. A. Sawatzky, and A. Damascelli, Science **347**, 282 (2015).

[39] V. M. Loktev, R. M. Quick, and S. G. Sharapov, Phys. Rep. **349**, 1 (2001).

[40] Y. Wang and A. Chubukov, Phys. Rev. B **91**, 195113 (2015).

[41] Y. Wang, D. F. Agterberg, and A. Chubukov, Phys. Rev. Lett. **114**, 197001 (2015).

[42] C. Wang, B. Giambattista, C. G. Slough, R. V. Coleman, and M. A. Subramanian, Phys. Rev. B **42**, 8890 (1990).

[43] I. Giaever, in *Superconductivity: Discoveries and Discoverers. Ten Physics Nobel Laureates Tell Their Story*, edited by K. Fossheim (Springer Verlag, Berlin, 2013), p. 53.

[44] M. Tinkham, *Introduction to Superconductivity* (Dover, Mineola, 2004).

[45] A. M. Gabovich, Fiz. Nizk. Temp. **18**, 693 (1992).

[46] A. M. Gabovich and A. I. Voitenko, Phys. Rev. B **55**, 1081 (1997).

[47] A. M. Gabovich and A. I. Voitenko, J. Phys.: Condens. Matter **9**, 3901 (1997).

[48] A. I. Voitenko and A. M. Gabovich, Fiz. Tverd. Tela **39**, 991 (1997).

[49] T. Ekino, A. M. Gabovich, and A. I. Voitenko, Fiz. Nizk. Temp. **34**, 515 (2008).

[50] A. M. Gabovich and A. I. Voitenko, Phys. Rev. B **75**, 064516 (2007).

[51] A. M. Gabovich and A. I. Voitenko, Physica C **503**, 7 (2014).

[52] A. M. Gabovich, M. S. Li, H. Szymczak, and A. I. Voitenko, Phys. Rev. B **87**, 104503 (2013).

[53] R. Comin, R. Sutarto, E. H. da Silva Neto, L. Chauviere, R. Liang, W. N. Hardy, D. A. Bonn, F. He, G. A. Sawatzky, and A. Damascelli, Science **347**, 1335 (2015).

[54] G. Campi, D. Innocenti, and A. Bianconi, J. Supercond. **28**, 1355 (2015).

[55] J. C. Phillips, A. Saxena, and A. R. Bishop, Rep. Prog. Phys. **66**, 2111 (2003).

[56] H. Alloul, J. Bobroff, M. Gabay, and P. J. Hirschfeld, Rev. Mod. Phys. **81**, 45 (2009).

[57] J. C. Phillips, Adv. Condens. Matter Phys. **2010**, 250891 (2010).

[58] N. Barišić, M. K. Chan, Y. Li, G. Yu, X. Zhao, M. Dressel, A. Smontara, and M. Greven, Proc. Nat. Acad. Sci. USA **110**, 12235 (2013).

[59] A. Shengelaya and K. A. Müller, Europhys. Lett. **109**, 27001 (2015).

[60] T. Honma and P. H. Hor, Physica C **509**, 11 (2015).

[61] X. Zhu, Y. Cao, J. Zhang, E. W. Plummer, and J. Guo, Proc. Nat. Acad. Sci. USA **112**, 2367 (2015).

[62] J. M. Tranquada, in *Lectures on the Physics of Strongly Correlated Systems XVII. Seventeenth Training Course in the Physics of Strongly Correlated Systems*, edited by A. Avella and F. Mancini (American Institute of Physics, Melville, 2013), p. 114.

[63] R. Daou, J. Chang, D. LeBoeuf, O. Cyr-Choinière, F. Laliberté, N. Doiron-Leyraud, B. J. Ramshaw, R. Liang, D. A. Bonn, W. N. Hardy, and L. Taillefer, Nature (London) **463**, 519 (2010).

[64] M. J. Lawler, K. Fujita, J. Lee, A. R. Schmidt, Y. Kohsaka, C. K. Kim, H. Eisaki, S. Uchida, J. C. Davis, J. P. Sethna, and E.-A. Kim, Nature (London) **466**, 347 (2010).

[65] E. H. da Silva Neto, P. Aynajian, R. E. Baumbach, E. D. Bauer, J. Mydosh, S. Ono, and A. Yazdani, Phys. Rev. B **87**, 161117(R) (2013).

[66] S. Sugai, Y. Takayanagi, N. Hayamizu, T. Muroi, R. Shiozaki, J. Nohara, K. Takenaka, and K. Okazaki, J. Phys.: Condens. Matter **25**, 475701 (2013).

[67] S. Jiang, H. S. Jeevan, J. Dong, and P. Gegenwart, Phys. Rev. Lett. **110**, 067001 (2013).

[68] S. Kasahara, H. J. Shi, K. Hashimoto, S. Tonegawa, Y. Mizukami, T. Shibauchi, K. Sugimoto, T. Fukuda, T. Terashima, A. H. Nevidomskyy, and Y. Matsuda, Nature (London) **486**, 382 (2012).

[69] S. Avci, O. Chmaissem, J. M. Allred, S. Rosenkranz, I. Eremin, A. V. Chubukov, D. E. Bugaris, D. Y. Chung, M. G. Kanatzidis, J.-P. Castellan, J. A. Schlueter, H. Claus, D. D. Khalyavin, P. Manuel, A. Daoud-Aladine, and R. Osborn, Nat. Commun. **5**, 3845 (2014).

[70] M. Vojta, Eur. Phys. J. Special Topics **188**, 49 (2010).

[71] E. Fradkin, S. A. Kivelson, M. J. Lawler, J. P. Eisenstein, and A. P. Mackenzie, Annu. Rev. Condens. Matter Phys. **1**, 153 (2010).

[72] E.-G. Moon and S. Sachdev, Phys. Rev. B **85**, 184511 (2012).

[73] B. Phillabaum, E. W. Carlson, and K. A. Dahmen, Nat. Commun. **3**, 915 (2012).

[74] V. Stanev and P. B. Littlewood, Phys. Rev. B **87**, 161122 (2013).

[75] R. M. Fernandes, A. V. Chubukov, and J. Schmalian, Nature Phys. **10**, 97 (2014).

[76] W. A. Atkinson, A. P. Kampf, and S. Bulut, New J. Phys. **17**, 013025 (2015).

[77] E. W. Carlson, S. Liu, B. Phillabaum, and K. A. Dahmen, J. Supercond. **28**, 1237 (2015).

[78] V. M. Loktev and Yu. G. Pogorelov, *Dopants and Impurities in High-Tc Superconductors* (Akademperiodika, Kiev, 2015).

[79] B. Mühlschlegel, Z. Phys. **155**, 313 (1959).

[80] W. S. Lee, I. M. Vishik, K. Tanaka, D. H. Lu, T. Sasagawa, N. Nagaosa, T. P. Devereaux, Z. Hussain, and Z.-X. Shen, Nature (London) **450**, 81 (2007).

[81] B. Keimer, S. A. Kivelson, M. R. Norman, S. Uchida, and J. Zaanen, Nature (London) **518**, 179 (2015).

[82] H. Won and K. Maki, Phys. Rev. B **49**, 1397 (1994).

[83] T. Ekino, A. M. Gabovich, M. S. Li, M. Pękała, H. Szymczak, and A. I. Voitenko, J. Phys.: Condens. Matter **23**, 385701 (2011).

[84] A. M. Gabovich, A. I. Voitenko, and M. Ausloos, Phys. Rep. **367**, 583 (2002).

[85] D. F. Agterberg and J. Garaud, Phys. Rev. B **91**, 104512 (2015).

[86] Y. Wang, D. F. Agterberg, and A. Chubukov, Phys. Rev. B **91**, 115103 (2015).

[87] A. Greco and R. Zeyher, Phys. Rev. B **70**, 024518 (2004).

[88] A. Barone and G. Paterno, *The Physics and Applications of the Josephson Effect* (John Wiley and Sons, New York, 1982).

[89] V. M. Krasnov, Phys. Rev. B **91**, 224508 (2015).

[90] H. B. Dwight, *Tables of Integrals and Other Mathematical Data* (The Macmillan Company, New York, 1961).

[91] I. O. Kulik and I. K. Yanson, *Josephson Effect in Superconducting Tunneling Structures* (Coronet, New York, 1971).

[92] E. L. Wolf, *Principles of Electron Tunneling Spectroscopy* (Oxford University Press, New York, 1985).

[93] M. Ledvij and R. A. Klemm, Phys. Rev. B **51**, 3269 (1995).

[94] Q. Li, Y. N. Tsay, M. Suenaga, R. A. Klemm, G. D. Gu, and N. Koshizuka, Phys. Rev. Lett. **83**, 4160 (1999).

[95] Y. Takano, T. Hatano, A. Fukuyo, A. Ishii, M. Ohmori, S. Arisawa, K. Togano, and M. Tachiki, J. Low Temp. Phys. **131**, 533 (2003).
[96] Yu. I. Latyshev, A. P. Orlov, A. M. Nikitina, P. Monceau, and R. A. Klemm, Phys. Rev. B **70**, 094517 (2004).
[97] R. A. Klemm, Phil. Mag. **85**, 801 (2005).
[98] J. R. Waldram, Rep. Prog. Phys. **39**, 751 (1976).
[99] T. Kitamura, T. Kashiwagi, T. Yamamoto, M. Tsujimoto, C. Watanabe, K. Ishida, S. Sekimoto, K. Asanuma, T. Yasui, K. Nakade, Y. Shibano, Y. Saiwai, H. Minami, R. A. Klemm, and K. Kadowaki, Appl. Phys. Lett. **105**, 202603 (2014).
[100] M. Ji, J. Yuan, B. Gross, F. Rudau, D. Y. An, M. Y. Li, X. J. Zhou, Y. Huang, H. C. Sun, Q. Zhu, J. Li, N. Kinev, T. Hatano, V. P. Koshelets, D. Koelle, R. Kleiner, W. W. Xu, B. B. Jin, H. B. Wang, and P. H. Wu, Appl. Phys. Lett. **105**, 122602 (2014).
[101] J. Mannhart and P. Chaudhari, Phys. Today **54**, 48 (2001).
[102] A. D. Darminto, H.-J. H. Smilde, V. Leca, D. H. A. Blank, H. Rogalla, and H. Hilgenkamp, Phys. Rev. Lett. **94**, 167001 (2005).
[103] F. Tafuri and J. R. Kirtley, Rep. Prog. Phys. **68**, 2573 (2005).
[104] F. Tafuri, D. Massarotti, L. Galletti, D. Stornaiuolo, D. Montemurro, L. Longobardi, P. Lucignano, G. Rotoli, G. P. Pepe, A. Tagliacozzo, and F. Lombardi, J. Supercond. **26**, 21 (2013).
[105] D. J. Scalapino, Phys. Rep. **250**, 329 (1995).
[106] A. I. Larkin and Yu. N. Ovchinnikov, Zh. É ksp. Teor. Fiz. **51**, 1535 (1966).
[107] A. M. Gabovich, M. S. Li, H. Szymczak, and A. I. Voitenko, in *Superconductors–Materials, Properties and Applications*, edited by A. Gabovich (InTech, Rijeka, Croatia, 2012), p. 289.
[108] C. Kurter, L. Ozyuzer, J. F. Zasadzinski, D. G. Hinks, and K. E. Gray, J. Supercond. **24**, 101 (2011).
[109] A. I. Voitenko and A. M. Gabovich, Fiz. Tverd. Tela **49**, 1356 (2007).
[110] T. Ekino, A. M. Gabovich, M. S. Li, M. Pękała, H. Szymczak, and A. I. Voitenko, J. Phys.: Condens. Matter **20**, 425218 (2008).
[111] M. H. Cohen, L. M. Falicov, and J. C. Phillips, Phys. Rev. Lett. **8**, 316 (1962).
[112] Yu. V. Kopaev, Trudy Fiz. Inst. Akad. Nauk SSSR **86**, 3 (1975).
[113] A. M. Gabovich, E. A. Pashitskii, and A. S. Shpigel, Fiz. Tverd. Tela **18**, 3279 (1976).
[114] S. N. Artemenko and A. F. Volkov, Zh. Éksp. Teor. Fiz. **87**, 691 (1984).
[115] A. M. Gabovich and A. I. Voitenko, Phys. Rev. B **56**, 7785 (1997).
[116] T. Ekino, Y. Sezaki, and H. Fujii, Phys. Rev. B **60**, 6916 (1999).
[117] Ø. Fischer, M. Kugler, I. Maggio-Aprile, and C. Berthod, Rev. Mod. Phys. **79**, 353 (2007).
[118] T. Ekino, A. M. Gabovich, M. S. Li, M. Pękała, H. Szymczak, and A. I. Voitenko, Phys. Rev. B **76**, 180503 (2007).
[119] A. M. Gabovich and A. I. Voitenko, Phys. Rev. B **52**, 7437 (1995).
[120] K. S. Aleksandrov and B. V. Beznosikov, Fiz. Tverd. Tela **39**, 785 (1997).
[121] M. Karppinen and H. Yamauchi, Mat. Sci. Eng. R **26**, 51 (1999).
[122] R. J. Cava, J. Am. Ceram. Soc. **83**, 5 (2000).
[123] T. Yoshida, M. Hashimoto, I. M. Vishik, Z.-X. Shen, and A. Fujimori, J. Phys. Soc. Jpn. **81**, 011006 (2012).
[124] K. Fujita, A. R. Schmidt, E.-A. Kim, M. J. Lawler, D. H. Lee, J. C. Davis, H. Eisaki, and S-i. Uchida, J. Phys. Soc. Jpn. **81**, 011005 (2012).
[125] S. Shapiro, P. H. Smith, J. Nicol, J. L. Miles, and P. F. Strong, IBM J. Res. Dev. **6**, 34 (1962).
[126] S. I. Vedeneev, B. A. Piot, and D. K. Maude, Phys. Rev. B **81**, 054501 (2010).
[127] V. M. Krasnov, A. Yurgens, D. Winkler, P. Delsing, and T. Claeson, Phys. Rev. Lett. **84**, 5860 (2000).
[128] V. M. Krasnov, A. E. Kovalev, A. Yurgens, and D. Winkler, Phys. Rev. Lett. **86**, 2657 (2001).
[129] M. Suzuki, T. Hamatani, K. Anagawa, and T. Watanabe, Phys. Rev. B **85**, 214529 (2012).
[130] M. Suzuki, R. Takemura, K. Hamada, M. Ohmaki, and T. Watanabe, Jpn. J. Appl. Phys. **51**, 010112 (2012).
[131] Th. Jacobs, S. O. Katterwe, H. Motzkau, A. Rydh, A. Maljuk, T. Helm, C. Putzke, E. Kampert, M. V. Kartsovnik, and V. M. Krasnov, Phys. Rev. B **86**, 214506 (2012).
[132] Ya. G. Ponomarev, E. B. Tsokur, M. V. Sudakova, S. N. Tchesnokov, M. E. Shabalin, M. A. Lorenz, M. A. Hein, G. Müller, H. Piel, and B. A. Aminov, Solid State Commun. **111**, 513 (1999).